Precambrian Research, 49 (1991) 301–327
Elsevier Science Publishers B.V., Amsterdam

Isotopic compositions of carbonates and organic carbon from upper Proterozoic successions in Namibia: stratigraphic variation and the effects of diagenesis and metamorphism

Alan J. Kaufman[a,1], J.M. Hayes[a], Andrew H. Knoll[b] and Gerard J.B. Germs[c]

[a]*Biogeochemical Laboratories, Departments of Geology and Chemistry, Indiana University, Bloomington IN 47405-5101, USA*
[b]*Botanical Museum, Harvard University, Cambridge MA 02138, USA*
[c]*J.C.I. Research Unit, P.O. Box 976, 1760 Randfontein, South Africa*

(Received July 25, 1989; revised and accepted July 11, 1990)

ABSTRACT

Kaufman, A.J., Hayes, J.M., Knoll, A.H. and Germs, G.J.B., 1991. Isotopic compositions of carbonates and organic carbon from upper Proterozoic successions in Namibia: stratigraphic variation and the effects of diagenesis and metamorphism. Precambrian Res., 49: 301–327.

The carbon isotope geochemistry of carbonates and organic carbon in the late Proterozoic Damara Supergroup of Namibia, including the Nama, Witvlei, and Gariep groups on the Kalahari Craton and the Mulden and Otavi groups on the Congo Craton, has been investigated as an extension of previous studies of secular variations in the isotopic composition of late Proterozoic seawater. Subsamples of microspar and dolomicrospar were determined, through petrographic and cathodoluminescence examination, to represent the "least-altered" portions of the rock. Carbon-isotopic abundances in these phases are nearly equal to those in total carbonate, suggesting that ^{13}C abundances of late Proterozoic fine-grained carbonates have not been significantly altered by meteoric diagenesis, although ^{18}O abundances often differ significantly. Reduced and variable carbon-isotopic differences between carbonates and organic carbon in these sediments indicate that isotopic compositions of organic carbon have been altered significantly by thermal and deformational processes, likely associated with the Pan-African Orogeny.

Distinctive stratigraphic patterns of secular variation, similar to those noted in other, widely separated late Proterozoic basins, are found in carbon-isotopic compositions of carbonates from the Nama and Otavi groups. For example, in Nama Group carbonates $\delta^{13}C$ values rise dramatically from -4 to $+5‰$ within a short stratigraphic interval. This excursion suggests correlation with similar excursions noted in Ediacaran-aged successions of Siberia, India, and China. Enrichment of ^{13}C ($\delta^{13}C > +5‰$) in Otavi Group carbonates reflects those in Upper Riphean successions of the Akademikerbreen Group, Svalbard, its correlatives in East Greenland, and the Shaler Group, northwest Canada. The widespread distribution of successions with comparable isotopic signatures supports hypotheses that variations in $\delta^{13}C$ reflect global changes in the isotopic composition of late Proterozoic seawater. Within the Damara basin, carbon-isotopic compositions of carbonates provide a potentially useful tool for the correlation of units between the Kalahari and Congo cratons.

Carbonates depleted in ^{13}C were deposited during and immediately following three separate glacial episodes in Namibia. The correspondence between ice ages and negative $\delta^{13}C$ excursions may reflect the effects of lowered sea levels; enhanced circulation of deep, cold, O_2-rich seawater; and/or the upwelling of ^{13}C-depleted deep water. Iron-formation is additionally associated with one of the glacial horizons, the Chuos tillite. Carbon-13 enriched isotopic abundances in immediately pre-glacial carbonates suggest that oceanographic conditions favored high rates of organic burial. It is likely that marine waters were stratified, with deep waters anoxic. A prolonged period of ocean stratification would permit the build-up of ferrous iron, probably from hydrothermal sources. At the onset of glaciation, upwelling would have brought ^{13}C-depleted and iron-rich deep water onto shallow shelves where contact with cold, oxygenated surface waters led to the precipitation of ferric iron.

[1] Present address: Botanical Museum, Harvard University, Cambridge, MA 02138, USA.

0301-9268/91/$03.50

Introduction

Phanerozoic marine carbonates record secular variations in seawater ^{13}C abundance (Keith and Weber, 1964; Veizer and Hoefs, 1976; Lindh, 1983; Holser, 1984; Holser et al., 1986). These are commonly interpreted as a consequence of changes in the relative rates of burial of organic and inorganic carbon in the sedimentary cycle (Schidlowski et al., 1975; Veizer et al., 1980; Scholle and Arthur, 1980; Holser et al., 1986). Recently, carbon-isotopic studies have revealed stratigraphic patterns of ^{13}C enrichment and fluctuation in carbonates from late Proterozoic basins (Knoll et al., 1986; Magaritz et al., 1986; Tucker, 1986a; Lambert et al., 1987; Aharon et al., 1987; Wang et al., 1987; Fairchild and Spiro, 1987) comparable in rate of change but greater in magnitude than those which characterize Phanerozoic basins. Integration of these results to establish a global pattern of secular variation during the late Proterozoic has been hindered by problems associated with the correlation of upper Proterozoic sedimentary sequences and by concerns that some of the isotopic variations may be of diagenetic origin or may reflect local rather than global conditions. Reduction of uncertainties will require (1) clear separation of primary variations from diagenetic or metamorphic overprints; (2) construction of isotopic records for multiple basins of comparable age with good local stratigraphic, paleoenvironmental, and petrographic control; and (3) secure correlation of multiple records in order to test hypotheses of global synchroneity of $^{13}C/^{12}C$ fluctuations. With these objectives in mind, we present results of a detailed study of the stable isotope geochemistry of carbonates and organic matter from the upper Proterozoic Damara Supergroup of Namibia. Insofar as carbon isotope signatures have proven to be valuable in the intrabasinal correlation of other upper Proterozoic successions (Knoll et al., 1986), it is reasonable to ask whether they might also help to unravel correlational problems between the Congo and Kalahari cratons of southwest Africa.

Geology

The Damara Supergroup (consisting of the Nama, Witvlei, Gariep, Mulden, Otavi, and Nosib groups) formed in response to Pan-African rifting (ca. 1100–1000 Ma) with subsequent spreading, subsidence, and marine transgression on the West Gondwanaland continent (Porada, 1989). On the Congo Craton (Fig. 1), initial rifting lead to the deposition of the Nosib Group; later subsidence and transgression lead to the development of a stable platform where the thick sequence of Otavi Group carbonates accumulated. Subsequent uplift in the northwestern part of the Damara Orogen, caused by subduction of the Kalahari Craton beneath the Congo Craton, resulted in deep erosion of Damaran and older rocks (Martin, 1965; Frets, 1969; Hedberg, 1979; Miller, 1983) and the consequent deposition of the Mulden Group as a molasse. On the Kalahari Craton (Fig. 1), Pan-African rifting and subsidence lead to the development of a passive continental margin and the subsequent accumulation of platform and basinal Gariep (Tankard et al., 1982) and Witvlei Group sediments. Marine transgression over the shallow water platforms resulted in deposition of the lower Nama Group. Subsequent infilling of the Nama basin with sediments shed from the rising Congo Craton in the north, or closure of the basin as a result of plate convergence lead to deposition of the upper Nama Group as a molasse (Germs, 1983).

Nama and Witvlei groups

The Nama Group has been divided into three lithologically distinct units, the Kuibis, Schwarzrand, and Fish River subgroups (Fig. 2). Due to lateral facies changes, the three subgroups of the Nama Group have been subdivided differently in the areas to the north and

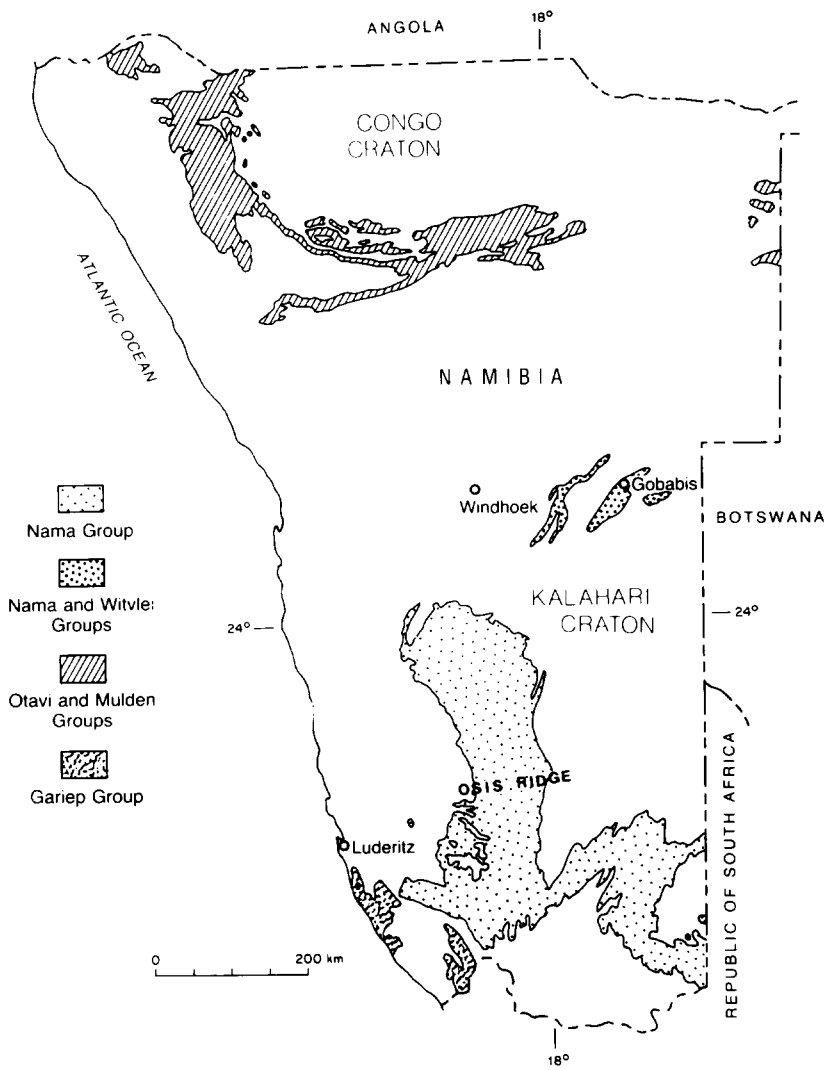

Fig. 1. Geologic map of the late Proterozoic Damara Supergroup in Namibia showing exposure of the Nama and Witvlei, Otavi and Mulden, and Gariep groups.

to the south of the Osis Ridge, a paleostructural feature that divided the developing Nama basin into two distinct parts (Germs, 1983; Fig. 1). The Nama Group is characterized by decreasing maturity of siliciclastic sediments from the Kuibis Subgroup at the base to the Fish River Subgroup at the top. Away from the Osis Ridge, the Kuibis Subgroup comprises two cycles of basal conglomerate followed by feldsphatic sandstone, orthoquartzite, shale, and limestone. Thick limestones and terrigenous sediments dominate the Schwarzrand Subgroup. The Fish River Subgroup consists predominantly of reddish, fluviatile sandstone with minor silty shales. West of Windhoek, marine carbonates of the Buschmannsklippe Formation and purportedly lacustrine limestones (Hegenberger, pers. comm., 1987), shales, and sandstones of the Court Formation, previously assigned to the Kuibis Subgroup (but not by Germs), are now recognized as the Witvlei Group (Hoffmann, 1989). The Witvlei Group has unconformable contacts with the Blaubeker tillite of the Nosib

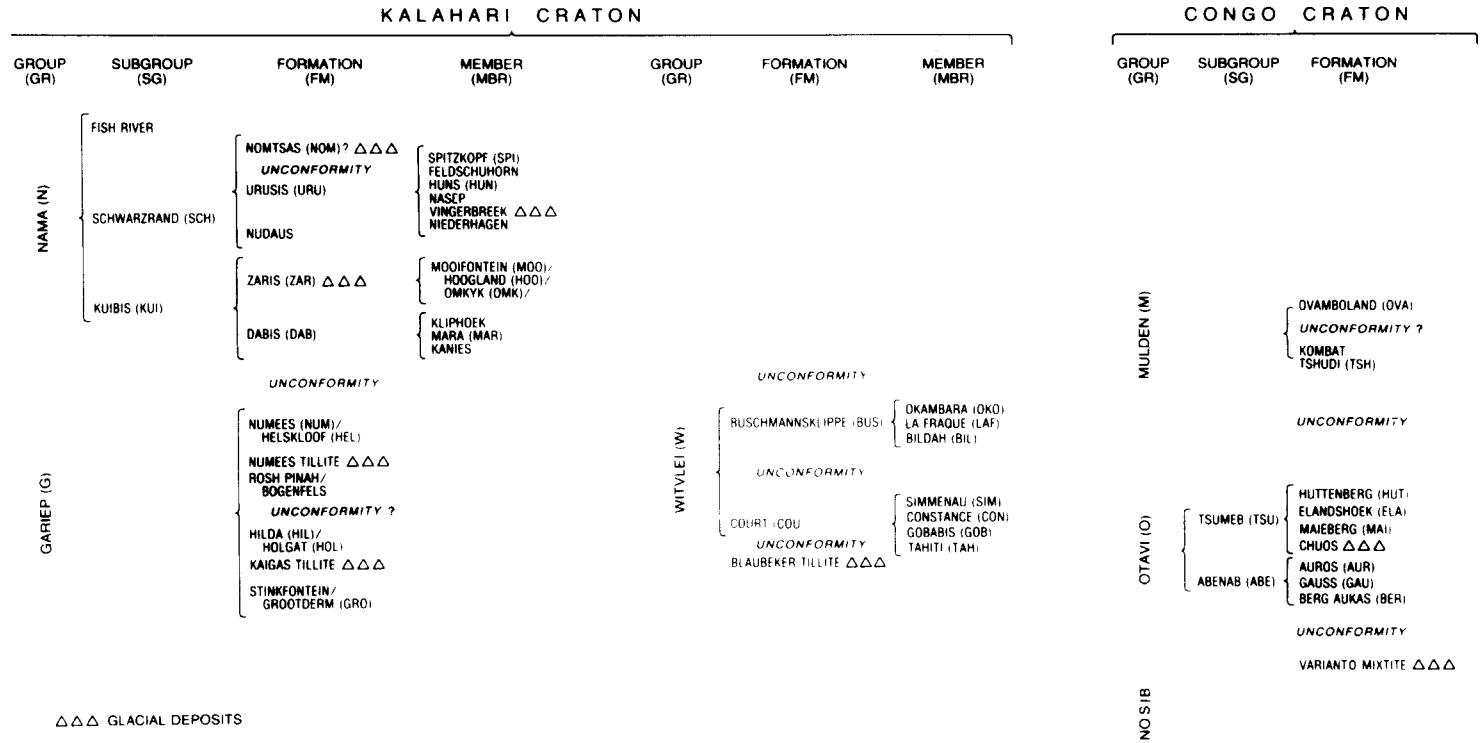

Fig. 2. Stratigraphy and generalized correlation among sections (after Hegenberger and Hoffmann, pers. comm., 1989 and modified from Miller, 1983). Abbreviations of headings and stratigraphic names which appear here correspond to those used in Table 1.

Group at its base and with the Dabis Formation of the Nama Group at its top (Germs, 1975). A major hiatus separates the sediments of the Buschmannsklippe and Court formations (Hoffmann, 1989).

The Nama Group contains an exceptional record of early invertebrate evolution. The Kuibis and Schwarzrand subgroups contain casts, molds and impressions of Ediacarangrade animals (Gürich, 1930, 1933; Richter, 1955; Glaessner, 1963, 1978, 1979; Pflug, 1966, 1970a,b, 1972, 1973; Germs, 1973a,b). Also occurring in the lower Nama Group are the oldest known examples of metazoan biomineralization (Germs, 1972a,b; Glaessner, 1984; Grant, 1990), possible calcareous algae (Grant et al., 1991), a dozen ichnotaxa (Germs, 1972c; Crimes and Germs, 1982), and a depauperate assemblage of organic-walled microfossils (Germs et al., 1986).

On paleontological evidence, the Kuibis and lower Schwarzrand subgroups are considered to be late Vendian (Valdaian) in age (Germs, 1972a,b; Crimes and Germs, 1982; Germs et al., 1986). The age of the uppermost Schwarzrand Subgroup (i.e., Nomtsas Formation) remains uncertain. Nomtsas strata are separated from lower and middle Schwarzrand rocks by a locally profound erosional discontinuity (Germs, 1983). Nomtsas sediments are not known to contain diagnostic Vendian or Cambrian body fossils, but do contain the trace fossils *Phycodes pedum* (Germs, 1972c) and *Diplichnites* (Crimes and Germs, 1982), which some workers take to indicate a Cambrian age of deposition (Crimes, 1987; Narbonne and Myrow, 1988). Paleomagnetic data suggest that the Nomtsas Formation and overlying Fish River Subgroup are younger than 600 Ma (Kröner et al., 1980; Crimes and Germs, 1982).

Available radiometric dates broadly corroborate ages suggested by paleontologic and paleomagnetic data. Detrital white micas in upper Schwarzrand sediments yield an age of approximately 630 Ma, whereas micas in younger Fish River sediments yield an age of approximately 530 Ma (Ahrendt et al., 1978). The post-tectonic Kuboos and Bremen igneous suites, which are intrusive into the Kuibis and Schwarzrand subgroups yield ages between 500 and 550 Ma (Allsopp et al., 1979; Rb–Sr whole rock isochron). These dates provide a minimum age of 500 Ma for the uppermost Schwarzrand Subgroup. Based on K–Ar age determinations of detrital white mica, Horstmann et al. (1990) narrowed the time of sedimentation of the upper Schwarzrand and Fish River subgroups to between 570 and 530–500 Ma.

Gariep Group

The Gariep Group is divided into a miogeosynclinal succession of carbonates, siliciclastic shelf sediments, and diamictites and a eugeosynclinal succession of volcanic rocks overlain by fine-grained terrigenous siliciclastic rocks (Martin, 1965; McMillan, 1968; Kröner, 1971; Tankard et al., 1982). The stratigraphy of this group is summarized in Fig. 2. The Stinkfontein Formation overlies the unfoliated Obib leucogranite, which has an age of approximately 950 ± 30 Ma (Welke et al., 1979). A whole rock Rb–Sr age of 719 ± 28 Ma (De Villiers, 1968) was obtained from a felsic lava situated below the Numees Formation diamictite. The possibility of a marked unconformity between the Numees and Hilda formations, and stratigraphic uncertainty of this felsite make it difficult to determine whether this age represents an approximate date for the glacial event or whether it corresponds to some unit lower in the section. The Numees Formation is overlain unconformably by the Nama Group (Kröner and Germs, 1971).

Otavi Group

The Otavi Group is divided into the Abenab and Tsumeb subgroups, the base of the latter defined by the tillite-bearing Chuos Formation (Fig. 2). The Abenab Subgroup is dominated by thick dolomitic sequences interbedded with

thin limestones and local calcareous sandstones and shales. Similarly, above the Chuos Formation, the Tsumeb Subgroup consists of a thick sequence of massive and well-bedded dolomites and limestones (Hedberg, 1979; Mason, 1981).

The Otavi Group is characterized by marker beds and stromatolitic horizons that can be traced over distances of at least 500 km (Kruger, 1969; Hedberg, 1979). The stromatolites *Baicalia* aff., *B. rara* and *Conophyton ressoti* occur in the lower Otavi Group, and *Conophyton* sp. is reported from the upper Otavi Group (Hedberg, 1979).

Radiometric dates on lavas of the Naauwpoort Formation place sharp limits on the timing of initial Otavi sedimentation. The Naauwpoort Formation occurs at the top of the Nosib Group which underlies the Otavi Group. These groups are typically separated by a pronounced unconformity; however, in the central Damara Belt, the Nosib sequence appears to be transitional upwards into the lower Otavi sequence (Smith, 1961; Jacob, 1974). Zircons from two groups of samples from quartz porphyry lavas near the base of the Naauwpoort Formation give U–Pb ages of 728 ± 40 and 750 ± 65 Ma (Miller and Burger, 1983), thus providing a reliable maximum age limit for the onset of Otavi deposition.

Mulden Group

The Mulden Group is divided into the Tshudi, Kombat, and Ovamboland Formation (Fig. 2). This group is composed of a thick sequence of feldspathic quartzite, arkose, greywacke, shale, and minor carbonate which paraconformably to slightly disconformably overlies the Otavi Group in the east (Söhnge, 1964). In the west and northwest, the Mulden Group becomes markedly discordant over older stratigraphic units, filling deeply incised paleovalleys in Otavi, Swakop and Nosib rocks, as well as pre-Damara basement (Martin, 1965; Frets, 1969; Hedberg, 1979; Miller, 1983).

No detailed paleontological studies on the Mulden Group have been carried out. Thus far only remains of the ribbon-like macrofossil *Vendotaenia* (Vidal, pers. comm., 1980) have been found in the upper Mulden Ovamboland Formation (Fig. 2). The Mulden and underlying Otavi successions were deformed during the second folding phase of the Pan-African Orogeny (ca. 600 Ma; Welke et al., 1979; Lombaard et al., 1986), setting a younger age limit on their deposition.

Lithologic correlations

In order to unravel the complex sedimentary and tectonic history of the Damara Orogen, it is necessary to determine the relative ages of the molasse (represented by the Mulden and upper Nama groups) and carbonate (represented by the lower Nama, Witvlei, Otavi, and Gariep groups) sequences. Because sediments deposited on the Kalahari and Congo cratons are not in stratigraphic contact, glaciogenic rocks have typically been used to correlate these upper Proterozoic successions.

McMillan (1968) and Hoffmann (1989) believe that the tillites in the Numees Formation of the Gariep Group are younger than the Chuos Formation tillite of the Otavi Group (Figs. 2 and 3). These workers suggest a correlation of the Kaigas tillite at the base of the Hilda Formation with the Chuos tillite. Kröner (1971) considered a putative tillite in the lower Schwarzrand Subgroup of the Nama Group to correlate with the Chuos tillite, implying that the Kuibis Subgroup is correlative with the Abenab Subgroup. This correlation further implies that Nama Group carbonates occurring below the Fish River Subgroup are coeval with carbonates in the Tsumeb Subgroup and that the Fish River Subgroup is equivalent to the Mulden Group. Further complicating the issue, Germs (1974) suggested that the base of the Mulden Group is older than the Nama

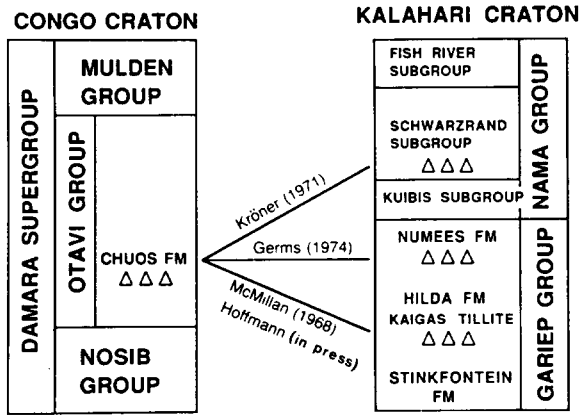

Fig. 3. Published interpretations of correlations among tillites in upper Proterozoic units on the Congo and Kalahari cratons.

Group (Fig. 2), and that the lower Schwarzrand diamictite represents a minor glaciation, not correlative with the widespread glacial event represented by the Chuos tillite. Instead, the tillite in the Numees Formation was considered by Germs (1974) to be equivalent to the Chuos tillite. Recent field observations by Germs and Hoffmann suggest that the Buschmannsklippe Formation of the Witvlei Group may be a nearshore equivalent of the lower Numees Formation (Hoffmann, 1989). This correlation implies that the hiatus which exists between the Buschmannsklippe and Court formations (Hoffmann, 1989) is time equivalent to the Numees tillite (possibly including upper Court sediments), and that the existing Court Formation and underlying Blaubeker tillite correlate with the Hilda Formation and Kaigas tillite, respectively (Fig. 2).

From radiometric ages of Damara granites, the age of the mineralization event in the Tsumeb mine, and from tectonic extrapolations, Miller (1983) came to the same conclusion as Germs (1974) concerning the ages of the Otavi, Mulden and Nama groups. Further, the correlation of Nama and Mulden sediments has been supported by paleomagnetic results (Kröner et al., 1980).

Methods

Sample selection and preparation

Effects of diagenesis have been evaluated by comparison of carbon- and oxygen-isotopic compositions of total carbonate with those of subsamples of microspar and dolomicrospar, determined through petrographic and cathodoluminescence (CL) examination to represent the "least-altered" portions of the rock (cf. Fairchild et al., 1988). Carbon-isotopic compositions of total organic carbon (TOC) were also determined to further evaluate diagenetic to metamorphic alteration of isotopic abundances. Field specimens for the Gariep, Nama, and Witvlei groups were collected by A.H.K., J. Compton, G.J.B.G., M.V. von Veh, and W. Hegenberger. Core specimens from the Otavi and Mulden groups were generously provided from boreholes drilled by the Tsumeb Corporation. The 76 outcrop and 66 core samples were split into two portions. The first portion was cleaned, fragmented, etched, and ground (Wedeking et al., 1983) for whole-rock analyses. The second portion was cut so that two mirror-image faces were exposed from which a polished thin section, for petrographic analysis, and thick section ($\sim$90 μm), for cathodoluminescence examination and detailed microsampling, were prepared. Matching of the two sections allowed direct correlation of textural components described from the thin section and physically isolated from the thick section. To determine the carbonate mineralogy, chips adjacent to the petrographic sections were stained with potassium ferricyanide and Alizarin red S (Dickson, 1966). Carbonate mineralogy of 30 sample powders was determined by X-ray diffraction.

Petrographic and cathodoluminescence (CL) examination

Luminescence in sedimentary carbonates is commonly activated by Mn^{2+} concentrations

of approximately 100 ppm and quenched by Fe^{2+} concentrations greater than 10,000 ppm (Hemming et al., 1989). Manganese enrichment is often the result of meteoric diagenesis of marine carbonates while iron enrichment may result from the dissolution and reprecipitation of carbonate during surfical weathering. A Nuclide Luminoscope (ELM-2B) set between 14–16 kV and 80–100 μA under a vacuum of approximately 50 mtorr was used in the CL examination of highly polished thick sections. Thick sections were photographed during CL examination.

Microsampling and isotopic analysis

Various carbonate phases were isolated from the thick sections by binocular observation of the sample and control of a low-speed drill with a 1.0 mm cobalt-steel rod ground to a sharp triangular point. The resulting fine powder was collected for subsequent isotopic analysis. Care was taken to avoid sampling areas near cross-cutting, late stage carbonate veins, weathered zones with abundant iron-rich clays and hematite, and zones where fine-grained microspar was intimately intermixed with coarse-grained sparry phases.

Carbonate powders were treated with H_3PO_4 ($\rho \geq 1.89$ g ml^{-1}) at 50°C for 48 h (Wachter and Hayes, 1985) to produce CO_2. For determination of the abundance and isotopic composition of TOC, powdered 50–250 mg samples were placed in Vycor tubes (9×150 mm) and repeatedly acidified (cold and hot, concentrated HCl) and washed to remove all carbonate. Cupric oxides was mixed with dried, decalcified samples in the same Vycor tubes. The tubes were evacuated, sealed, and heated at 850°C for 2 h. Recovery and purification of CO_2 formed by combustion of organic matter allowed both quantitative and isotopic analysis. Isotopic compositions of CO_2 were determined by conventional mass spectrometric techniques (Santrock et al., 1985) and are expressed relative to the PDB standard: $\delta = [(R_x/R_{PDB}) - 1] \times 10^3$, where $R = {}^{13}C/{}^{12}C$ or ${}^{18}O/{}^{16}O$ and the subscript x designates the sample. Fractionation factors employed for calculation of ^{18}O abundances in calcite and dolomite based on analyses of CO_2 prepared at 50°C were 1.00925 (McCrea, 1950; Wachter and Hayes, 1985) and 1.01066 (Rosenbaum and Sheppard, 1986), respectively.

Kerogens were extracted from six powdered samples by repeated treatment with cold HCl and HF, each for 24 h. Samples were acidified a third time with hot HCl to remove fluoride-bearing minerals possibly formed during treatment with HF. The residual kerogens were washed with deionized water until solutions reached neutrality. Wet kerogens were freeze-dried and subsequently analyzed for H/C ratios using a Carlo Erba elemental analyzer (Model 1106).

Petrography and cathodoluminescence

Nama Group

Nama Group limestones are finely-laminated, massive, oolitic, peloidal, and/or skeletal. These limestones are typified by mosaics of calcite microspar (10–50 μm; Fig. 4a) with abundances of sparry calcite (≥ 50 μm) ranging from ≤ 1 to 85%. An acicular carbonate cement is preserved in four samples as compressed bundles floating in a microspar matrix or as rows, growing tangentially on wavy, anastomosing laminations, concentrated along a single horizon (Fig. 4b). Many of the limestones have undergone partial dissolution as indicated by the common presence of stylolites. Organic matter is typically concentrated along these dissolution fronts. The presence of iron-rich clays and hematite in many samples is evidence of recent, surficial alteration of carbonate (Fig. 4c).

Calcite microspar in samples from the Nama Group is predominantly non-luminescent (see

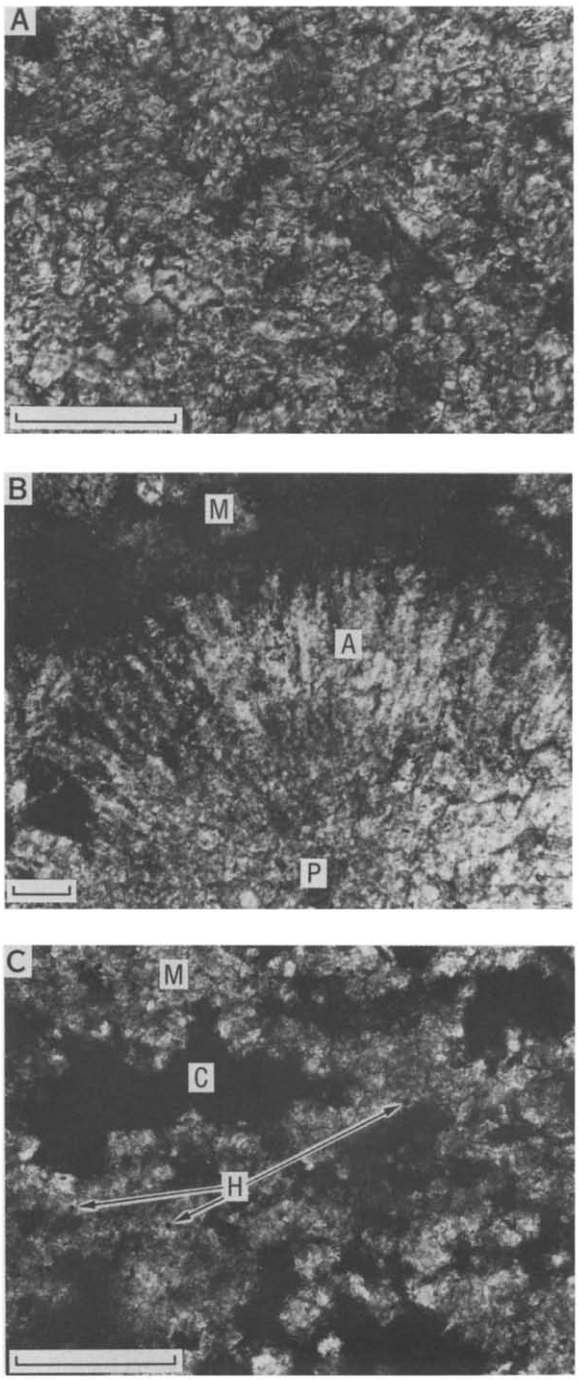

Fig. 4. Photomicrographs of Nama Group limestones taken in crossed polarized light. A. calcite microspar (sample SH 12). B. Fibrous, botryoidal carbonate cement (*A*) with randomly oriented needles on peloid (*P*) in a groundmass of calcite microspar (*M*; sample KO 138). C. calcite microspar (*M*) containing abundant iron-rich clays (*C*) and hematite (*H*; sample KM 1). Scale bars = 0.1 mm.

Fig. 5). In contrast, sparry calcite is always luminescent in these samples. Recently several authors (Sandberg, 1983; Tucker, 1983, 1985, 1986b; Fairchild and Spiro, 1987; Zempolich et al., 1988) have suggested that primary carbonate precipitates in late Proterozoic oceans were commonly aragonite. The absence of original aragonitic textures in late Proterozoic fine-grained carbonates (which retain high Sr contents) suggests that these precipitates have been subsequently neomorphosed to calcite microspar (Tucker, 1985, 1986b; Fairchild and Spiro, 1987; Swett and Knoll, 1989; Grant, 1990). Neomorphism of aragonite to calcite microspar probably occurred under the influence of marine solutions. It appears likely that later diagenesis under the influence of meteoric solutions yielded calcite microspar with variable luminescence.

Witvlei Group

Witvlei Group carbonates are finely-laminated, microbially-laminated, massive, oolitic, peloidal, and/or stromatolitic. These carbonates are primarily composed of calcite microspar, similar to Nama Group carbonates, with variable abundances of sparry calcite (ranging from 5 to 60%). Notably, Witvlei samples contain higher abundances of iron-rich clays and hematite than Nama samples.

Otavi Group

In contrast to Nama and Witvlei samples, petrographic and CL examination of Otavi Group dolomites and limestones, collected from core materials, suggests that these have not been strongly affected by either meteoric diagenesis or surficial weathering. These carbonates are composed of mosaics of fine-grained dolomicrospar and microspar (10–50 μm; Fig. 6a). Most samples contain less than 15% of sparry phases, which commonly occur as fracture-filling cements. Notable exceptions are the medium- to coarse-grained, foliated

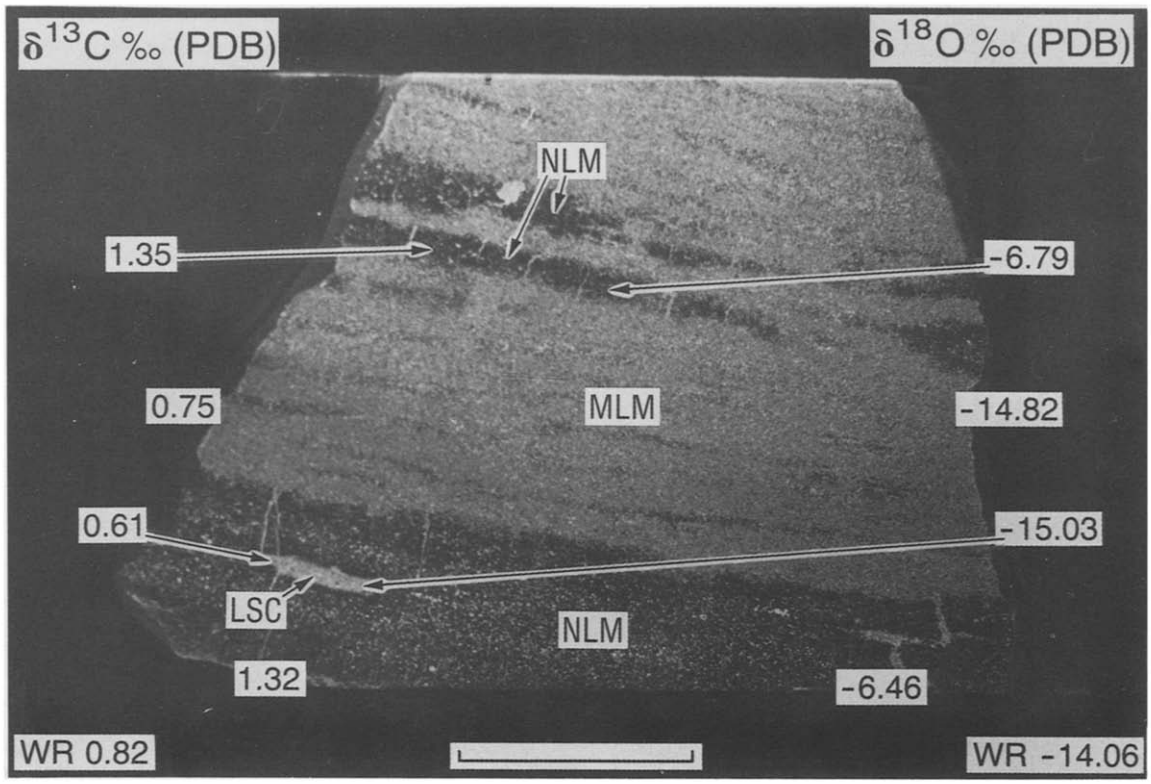

Fig. 5. Photograph of a highly polished thick section (approximately 90 μm) of sample SH 12 under cathodolumninescence. Carbon- and oxygen-isotopic compositions of non-luminescent microspar (*NLM*), moderately luminescent microspar (*MLM*), luminescent sparry calcite (*LSC*), and whole rock carbonate (*WR*) are shown. Scale bar = 1 cm.

iron-rich dolomites of the Maieberg and Berg Aukas formations (Fig. 6b). Medium-grained, disseminated pyrite euhedra are ubiquitous in these foliated dolomites as well as in the microbially-laminated dolomites of the Huttenberg and Elandshoek formations. Cherty cements commonly occur in pore spaces between anastomosing laminations in these fine-grained dolomites (Fig. 6c). No oolitic, peloidal, or skeletal textures were noted.

Mulden Group

Most samples taken from cores drilled into the molasse sediments of the Mulden Group consist of massive or finely-laminated siltstones and sandstones with minor amount ($\leq 10\%$) of calcitic cement. Medium- to coarse-grained pyrite is ubiquitous in these samples either as disseminated euhedra or as coarse lenses. A fibrous chert cement is closely associated with pyrite in a number of these samples. Relatively pure, massive or finely-laminated limestones and dolomites do occur in the Tshudi and Ovamboland formations, but are rare, and are typically medium- to coarse-grained and/or foliated or partly silicified.

Gariep Group

Silicification has also affected many of the outcrop samples collected from the Gariep Group. Fibrous chert cements and chert veins are evident in this sections of some of these samples. The massive, laminated, or stromatolitic limestones and dolomites are typically weathered, containing variable amounts of

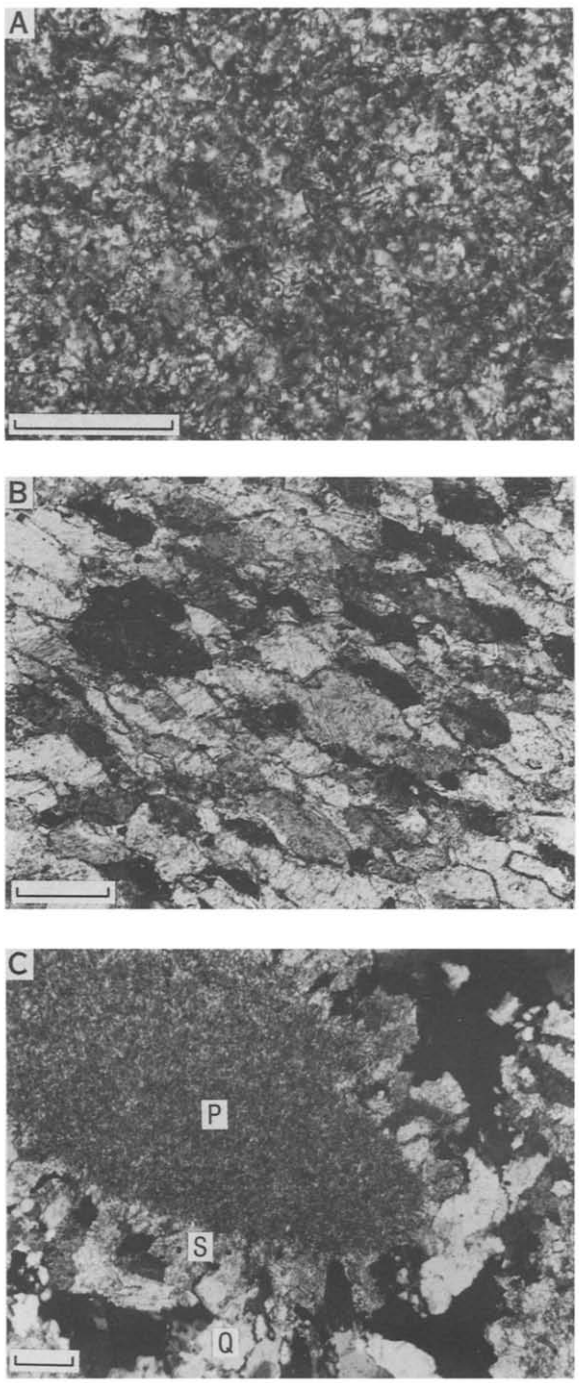

Fig. 6. Photomicrographs of Otavi Group dolomites taken in crossed polarized light. A. Dolomite microspar (sample AB50 260). B. Foliated carbonate (sample KH1 173). C. Cherty cement (*Q*) surrounding isopachous spar cement (*S*) and peloid (*P*) of dolomicrospar (sample AB 50 699). Scale bars = 0.1 mm.

iron-rich clays and hematite. Carbonate samples are both coarse-grained and foliated.

Isotopic analyses

Carbonates

Abundances and isotopic compositions of carbonates and organic carbon are listed in Table 1. To illustrate the heterogeneity within a single sample (SH 12), isotopic compositions of variably luminescent subsamples and of whole-rock (WR) carbonate are presented in Fig. 5. Microsamples were prepared from non-luminescent microspar (NLM), moderately luminescent microspar (MLM), and luminescent sparry calcite (LSC). In thin section, carbonate crystals in NLM are slightly finer-grained than carbonate crystals in MLM. Further, NLM has a relatively greater abundance of organic carbon relative to MLM. There is no variation in abundance of iron-rich clays or hematite between the two zones, but $\delta^{13}C$ and $\delta^{18}O$ ratios vary strongly. Non-luminescent microspar is enriched by 0.5, 0.6, and 0.7‰ in ^{13}C and 7.4, 8.2, and 8.4‰ in ^{18}O over WR, MLM, and LSC, respectively. Carbonate cements formed during meteoric diagenesis are typically depleted in carbon-13 and oxygen-18 (Gross, 1964: Veizer, 1978, 1983; Brand and Veizer, 1980, 1981). Therefore, the most enriched isotopic compositions (determined from NLM and isolated in this study) should most nearly reflect the isotopic compositions of primary marine precipitates.

Isotopic abundances in NLM and whole-rock carbonate are compared in Fig. 7. On average, NLM is enriched in ^{13}C relative to whole-rock carbonate by only 0.3‰. The NLM–WR carbon-isotopic difference is less than 0.5‰ in 70% of the cases and less than 1‰ in 98% of the cases. In similar studies, Fairchild and Spiro (1987) determined $\delta^{13}C$ ratios of NLM phases in late Precambrian carbonates from NE Spitsbergen and found that these were similar to $\delta^{13}C$ ratios of whole-rock samples from

TABLE I

Damara Supergroup, Namibia: Abundances and isotopic compositions[1]

Sample	GR	SG	FM	MBR	Lithology	% Carb	$\delta^{13}C_{WR}$ (‰,PDB)	$\delta^{13}C_{NLM}$ (‰,PDB)	$\delta^{18}O_{WR}$ (‰,PDB)	$\delta^{18}O_{NLM}$ (‰,PDB)	TOC (mgC/g)	$\delta^{13}C_{TOC}$ (‰,PDB)
SN 67	N	SCH	NOM		Silicified lms.	81.0	−5.71	−3.59	−2.52	0.49	0.34	−22.03
SN 72	N	SCH	NOM		Pelmicrite	47.3	2.40	2.05	−8.67	−8.29	0.05	−23.82
SN 75	N	SCH	NOM		Micrite	84.9	1.80	1.90	−9.36	−9.42	0.09	−25.30
SN 77	N	SCH	NOM		Sparmicrite	89.5	1.11	1.35	−11.15	−11.19	0.04	−21.88
SN 78	N	SCH	NOM		Sparite	91.2	1.08	0.57	−11.08	−7.29	0.09	−24.31
SN 80	N	SCH	NOM		Pelmicrite	92.5	1.05	1.45	−12.33	−8.10	0.37	−21.40
SN 81	N	SCH	NOM		Sparmicrite	91.0	1.32	1.55	−10.93	−14.02	0.17	−19.72
SS 16	N	SCH	URU	SPI	Sparmicrite	93.1	0.50	1.38	−11.60	−7.10	0.35	−25.44
SS 17	N	SCH	URU	SPI	Laminated lms.	92.0	1.73	1.83	−8.06	−6.23	0.43	−25.27
SS 18	N	SCH	URU	SPI	Micrite	93.5	2.10	1.79	−9.72	−7.64	0.36	−24.62
SH 12	N	SCH	URU	HUN	Laminated lms.	90.6	0.82	1.32	−14.00	−6.40	0.32	−25.62
SH 13	N	SCH	URU	HUN	Laminated lms.	93.9	0.99	1.46	−11.93	−8.73	0.46	−27.35
SH 14	N	SCH	URU	HUN	Laminated lms.	96.2	1.82	2.34	−8.22	−6.76	0.57	−26.18
SH 15	N	SCH	URU	HUN	Laminated lms.	90.3	−0.14	0.74	−12.02	−10.28	0.34	−26.70
SH 33	N	SCH	URU	HUN	Oolitic lms.	91.4	1.22	1.27	−8.06	−8.05	0.15	−20.85
SH 36	N	SCH	URU	HUN	Massive lms.	95.0	1.70	2.11	−11.58	−10.66	0.24	−20.22
SH 39	N	SCH	URU	HUN	Mottled lms.	93.2	1.85	2.58	−8.47	−8.09	0.47	−21.65
SH 41	N	SCH	URU	HUN	Sparmicrite	93.8	1.88	1.86	−10.18	−9.71	0.18	−21.03
SH 43	N	SCH	USU	HUN	Sparmicrite	95.3	1.21	n.d.	−9.52	n.d.	0.22	−22.49
SH 46	N	SCH	URU	HUN	Micsparite	97.2	1.44	1.41	−7.81	−6.97	0.27	−21.29
SH 48	N	SCH	URU	HUN	Micsparite	92.5	2.56	2.21	−8.09	−6.70	0.26	−21.03
SH 49	N	SCH	URU	HUN	Laminated lms.	11.0	1.57	1.64	−7.51	−6.36	0.34	−21.79
SH 51	N	SCH	URU	HUN	Biosparmicrite	91.5	1.77	2.17	−9.41	−8.77	0.61	−20.20
SH 54	N	SCH	URU	HUN	Massive lms.	90.4	1.46	1.63	−8.65	−6.17	0.33	−21.15
SH 56	N	SCH	URU	HUN	Laminated lms.	92.7	1.85	1.91	−6.26	−6.38	0.40	−20.68
SH 57	N	SCH	URU	HUN	Oomicrite	96.9	2.42	2.51	−8.18	−7.39	0.28	−20.16
KS 142	N	KUI	ZAR		Sparmicrite	91.5	2.70	2.76	−8.01	−6.63	0.10	−24.75
KS 145	N	KUI	ZAR		Sparmicrite	85.1	2.52	2.98	−9.80	−6.84	0.10	−24.10
KMO 5	N	KUI	ZAR	MOO	Micrite	91.2	−1.24	−0.68	−13.25	−13.84	0.48	−26.56
KMO 6	N	KUI	ZAR	MOO	Laminated lms.	85.8	−1.72	0.13	−9.86	−11.54	0.69	−25.82
KMO 8	N	KUI	ZAR	MOO	Oomicrite	96.4	0.24	n.d.	−11.74	n.d.	0.57	−24.90
KMO 92	N	KUI	ZAR	MOO	Micrite	68.2	4.79	n.d.	−13.05	n.d.	0.23	−23.93
KMO 93	N	KUI	ZAR	MOO	Micrite	91.0	4.32	4.22	−11.36	−10.57	0.70	−26.90
KMO 94	N	KUI	ZAR	MOO	Micrite	89.9	5.15	5.21	−11.22	−10.72	0.39	−26.09
KMO 95	N	KUI	ZAR	MOO	Oosparmicrite	81.1	4.34	5.00	−11.38	−11.19	0.40	−25.56
KMO 115	N	KUI	ZAR	MOO	Biosparmicrite	94.4	6.30	6.55	−9.87	−8.93	0.50	−25.45
KMO 116	N	KUI	ZAR	MOO	Biosparmicrite	91.5	5.51	5.34	−11.48	−11.70	0.20	−23.02
KMO 117	N	KUI	ZAR	MOO	Sparmicrite	94.7	4.86	4.99	−9.20	−8.17	0.16	−23.78
KMO 118	N	KUI	ZAR	MOO	Oomicrite	95.3	3.17	3.55	−8.58	−7.17	0.31	−25.22
KH1 24	N	KUI	ZAR	HOO	Sparmicrite	87.6	4.96	5.67	−8.96	−9.12	0.37	−21.96
KH1 25	N	KUI	ZAR	HOO	Micsparite	93.5	2.60	2.58	−6.45	−4.41	0.12	−22.38
KMO 114	N	KUI	ZAR	OMK	Oomicsparite	93.6	2.23	3.08	−7.37	−5.53	0.01	−23.60
KO 119	N	KUI	ZAR	OMK	Micspartie	94.9	5.42	5.81	−9.84	−8.96	0.54	−23.06
KO 138	N	KUI	ZAR	OMK	Biosparmicrite	81.3	0.65	1.48	−9.11	−6.49	0.17	−25.51
KO 139	N	KUI	ZAR	OMK	Biomicrite	92.0	2.14	2.44	−8.46	−8.59	0.06	−24.88
KO 140	N	KUI	ZAR	OMK	Sparmicrite	94.1	1.91	2.22	−8.76	−8.21	0.14	−23.66
KO 141	N	KUI	ZAR	OMK	Sparmicrite	93.6	2.23	n.d.	−7.37	n.d.	0.09	−23.60
KM 1	N	KUI	DAB	MAR	Algal laminite	97.9	−3.29	−2.97	−5.36	−4.04	0.90	−27.74
KM 2	N	KUI	DAB	MAR	Sparmicrite	94.8	−6.20	−6.09	−6.80	−5.82	0.29	−28.12
KM 3	N	KUI	DAB	MAR	Micrite	95.1	−5.18	−5.07	−3.10	−2.89	0.53	−31.50
KM 4	N	KUI	DAB	MAR	Algal laminite	95.0	−4.09	−3.99	−5.43	−5.45	0.80	−29.00

TABLE 1 (continued)

Sample	GR	SG	FM	MBR	Lithology	% Carb	$\delta^{13}C_{WR}$ (‰,PDB)	$\delta^{13}C_{NLM}$ (‰,PDB)	$\delta^{18}O_{WR}$ (‰,PDB)	$\delta^{18}O_{NLM}$ (‰,PDB)	TOC (mgC/g)	$\delta^{13}C_{TOC}$ (‰,PDB)
KM 111	N	KUI	DAB	MAR	Micsparite	87.1	−1.96	−1.74	−12.26	−10.31	0.44	−26.00
KM 113	N	KUI	DAB	MAR	Algal laminite	93.3	−1.52	−2.24	−8.83	−6.31	0.98	−24.67
203	W	BUS	OKA		Stromatolite	80.0	−2.92	−2.78	−5.34	−4.49	0.03	−24.54
407	W	BUS	OKA		Impure lms.	84.6	−3.91	n.d.	−0.86	n.d.	0.18	−24.32
393	W	BUS	OKA		lms./Cong.	79.7	−4.60	−4.64	−3.86	−3.79	0.21	−20.28
357	W	BUS	LAF		Impure lms.	34.5	−5.72	−5.46	−11.76	−12.07	0.16	−24.71
188	W	BUS	BIL		Algal laminite	88.5	−3.74	−3.72	−6.43	−5.70	n.d.	n.d.
449	W	BUS	BIL		Algal laminite	95.2	−3.17	−3.92	−6.95	−6.45	0.05	−23.36
159	W	COU	SIM		Stromatolite	74.9	1.73	1.44	−3.71	−2.04	0.06	−24.24
153	W	COU	SIM		Oomicrite	87.3	2.57	n.d.	−0.33	n.d.	0.10	−21.62
458	W	COU	CON		Impure lms.	88.0	−2.59	n.d.	−3.49	n.d.	0.06	−22.84
399	W	COU	GOB		Laminated lms.	86.5	−1.55	n.d.	−13.65	n.d.	0.12	−31.64
400	W	COU	GOB		Laminated lms.	84.5	−2.07	−1.92	−8.38	−9.02	1.15	−31.79
134	W	COU	GOB		Laminated lms.	78.1	−3.46	−2.83	−1.63	−1.82	0.20	−33.37
460	W	COU	GOB		Stromatolite	97.8	1.86	2.12	−2.84	−1.36	1.20	−27.32
AP39 436	O	TSU	HUT	T8	Dolosparmicrite	93.6	1.15	1.83	−4.24	−1.50	7.13	−24.78
S64 300	O	TSU	HUT	T8	Dolomicrite	50.0	2.24	n.d.	−6.50	n.d.	0.14	−16.26
KO4 238	O	TSU	HUT	T8	Algal laminite	84.4	1.59	1.37	−8.74	−8.66	11.68	−23.80
KO4 276	O	TSU	HUT	T8	Algal laminite	48.0	0.27	−0.42	−3.73	−3.07	8.29	−25.03
OV18A 615	O	TSU	HUT	T8	Dolosparmicrite	62.5	3.54	4.10	−8.91	−8.43	0.18	−15.99
AB50 257.5	O	TSU	HUT	T7	Dolomicrite	32.0	8.00	n.d.	−8.64	n.d.	2.14	−13.86
AB50 260	O	TSU	HUT	T7	Dolomicrite	71.6	6.59	n.d.	−9.02	n.d.	0.53	−15.01
AB50 261	O	TSU	HUT	T7	Dolomicrite	79.9	7.34	7.39	−8.82	−9.29	0.95	−14.13
AB50 263	O	TSU	HUT	T7	Dolomicrite	75.6	7.56	n.d.	−8.21	n.d.	4.88	−14.56
AB50 309	O	TSU	HUT	T7	Dolomicrite	79.1	9.17	8.88	−5.03	−5.00	1.46	−10.72
AB50 320	O	TSU	HUT	T7	Algal laminite	65.2	7.22	7.13	−4.85	−4.60	1.19	−12.37
AB50 438	O	TSU	HUT	T6	Dolomicrite	86.0	9.44	n.d.	−4.93	n.d.	1.16	−11.63
AB50 513	O	TSU	HUT	T6	Algal laminite	38.7	8.21	8.55	−6.47	−4.72	0.12	−21.43
AB50 602	O	TSU	HUT	T6	Algal laminite	96.6	2.78	2.37	−5.18	−4.59	0.15	−22.81
AB50 699	O	TSU	HUT	T5	Dolopelmicrite	81.0	1.92	2.47	−5.79	−5.51	0.11	−21.62
AB50 767	O	TSU	ELA	T5	Dolosparmicrite	93.8	2.41	n.d.	−5.77	n.d.	0.10	−18.82
AB50 898	O	TSU	ELA	T5	Dolomicrite	96.1	2.42	2.11	−5.66	−4.94	0.04	−17.80
NH5 53	O	TSU	ELA	T4	Dolosparmicrite	86.3	−0.02	0.46	−6.68	−6.22	0.11	−17.25
EH 1	O	TSU	ELA	T4	Dolosparmicrite	94.4	0.29	0.71	−7.64	−6.72	0.16	−22.62
EH 2	O	TSU	ELA	T4	Algal laminite	93.6	−1.26	−0.77	−7.98	−6.59	0.22	−23.40
EH 3	O	TSU	ELA	T3	Dolosparmicrite	95.6	−1.23	−1.12	−8.45	−7.92	0.10	−23.04
EH 4	O	TSU	ELA	T3	Dolosparmicrite	93.3	0.10	0.29	− 8.03	−7.49	0.20	−22.51
EH 8	O	TSU	ELA	T3	Dolosparmicrite	94.0	−0.55	−0.34	−7.35	−6.31	0.19	−16.91
EH 9	O	TSU	ELA	T3	Dolosparmicrite	93.1	−0.35	−0.15	−7.01	−5.73	0.20	−22.40
KH1 70	O	TSU	MAI	T2	Foldolomicrite	62.8	−3.12	−2.75	−10.36	−8.79	0.55	−23.00
KH1 173	O	TSU	MAI	T2	Fol. dolomicrite	84.6	−3.54	−3.18	−10.68	−10.08	0.46	−22.67
KH1 207	O	TSU	MAI	T2	Fol. dolomicrite	83.2	−4.16	−3.85	−10.58	−10.58	0.88	−23.41
KH1 255	O	TSU	MAI	T2	Fol. dolomicrite	21.4	−4.14	n.d.	−12.01	n.d.	0.55	−23.22
KH1 292	O	TSU	MAI	T2	Fol. dolomicrite	30.3	−4.79	n.d.	−13.93	n.d.	2.17	−23.20
KH1 377	O	TSU	MAI	T2	Fol. dolomicrite	38.9	−4.89	n.d.	−14.14	n.d.	0.93	−23.03
KH1 436	O	TSU	MAI	T2	Dolomicrite	28.2	−5.02	n.d.	−13.93	n.d.	0.50	−22.55
KH1 446	O	TSU	MAI	T2	Fol. dolomicrite	34.6	−4.60	n.d.	−12.76	n.d.	0.10	−22.77
NH6 117	O	TSU	MAI	T2	Brec. dolomicrite	87.1	−0.10	0.21	−5.73	−5.48	n.d.	n.d.
KH1 455	O	TSU	AUR		Dolomicrite	55.0	−3.12	n.d.	−10.72	n.d.	0.09	−24.04
KH1 531	O	TSU	GAU		Algal laminite	95.3	4.24	4.84	−8.93	−8.61	0.10	−22.61
HB3 132	O	ABE	GAU		Dolomicrite	88.8	5.02	n.d.	−3.64	n.d.	0.04	−15.99
HB3 154	O	ABE	GAU		Dolosparmicrite	93.7	5.81	6.78	−2.71	1.76	0.10	−14.90
37	O	ABE	BER		Fol. dolomicrite	55.6	3.08	n.d.	−4.49	n.d.	0.17	−10.42
38	O	ABE	BER		Algal laminite	69.1	2.85	2.67	−5.61	−5.94	0.20	−9.64
39	O	ABE	BER		Brec. dolomicrite	44.2	2.09	n.d.	−5.95	n.d.	0.38	−13.72

TABLE 1 (continued)

Sample	GR	SG	FM	MBR	Lithology	% Carb	$\delta^{13}C_{WR}$ (‰,PDB)	$\delta^{13}C_{NLM}$ (‰,PDB)	$\delta^{18}O_{WR}$ (‰,PDB)	$\delta^{18}O_{NLM}$ (‰,PDB)	TOC (mgC/g)	$\delta^{13}C_{TOC}$ (‰,PDB)
HU 62033	G		NUM		Shale	0.5	−4.65	n.d.	−13.15	n.d.	0.07	−24.89
HU 62034	G		NUM		Cherty lms.	86.8	−3.09	−3.20	−8.61	−13.49	0.11	−24.48
MV 453	G		NUM		Dolomicrite	74.3	4.15	4.82	−13.36	−13.12	0.23	−8.34
MV 458	G		NUM		Fol. Dolomicrite	88.1	4.00	4.48	−15.28	−15.28	0.63	−5.33
MV 635	G		HEL		Fol. limestone	60.9	0.75	1.24	−13.72	−11.81	1.35	−8.40
MV 773	G		HEL		Stromatolite	88.7	−4.28	n.d.	−13.75	n.d.	2.11	−13.22
MV 490	G		HIL		Sparmicrite	89.4	−1.71	−0.94	−10.46	−8.42	0.68	−14.13
MV 365	G		HIL		Limestone	82.8	7.93	8.76	−4.43	−4.31	0.71	1.31
MV 364	G		HIL		Dolosparite	64.1	4.67	5.54	−15.88	−15.77	1.72	−5.25
MV 900	G		GRO		Limestone	73.4	−2.90	−2.91	−4.43	−4.65	0.04	−22.69
AP39 310	M		TSH		Siltstone	0.8	−2.91	n.d.	−13.00	n.d.	1.00	−22.05
AP39 390	M		TSH		Siltstone	0.0	n.d.	n.d.	n.d.	n.d.	0.38	−19.58
KO4 187	M		TSH		Siltstone	0.8	5.06	n.d.	9.29	n.d.	4.10	−17.40
KO4 232	M		TSH		Siltstone	4.3	−0.28	n.d.	−11.54	n.d.	0.78	−21.75
OVST 2106	M		OVA		Siltstone	1.2	−3.04	n.d.	−2.80	n.d.	0.63	−20.97
OVST 2123	M		OVA		Silty lms.	62.3	−3.67	−3.83	−12.81	−13.12	0.36	−26.57
OVST 2125	M		OVA		Siltstone	17.6	−2.59	n.d.	−4.85	n.d.	0.61	−21.00
OVST 2154	M		OVA		Siltstone	7.1	−4.52	n.d.	−9.38	n.d.	0.63	−22.32
OVST 2992	M		OVA		Siltstone	15.2	−5.72	n.d.	−5.64	n.d.	12.15	−32.34
OVST 2994	M		OVA		Micrite	84.7	−2.18	−1.87	−12.84	−12.96	2.59	−31.93
OVST 2998	M		OVA		Quartzite	5.0	−8.27	n.d.	−12.09	n.d.	0.13	−26.44
OVST 3015	M		OVA		Siltstone	13.0	−5.68	−4.83	−10.97	−10.47	n.d.	n.d.
OVST 3298	M		OVA		Siltstone	16.8	−5.43	n.d.	−3.09	n.d.	1.81	−29.85
OVST 3299	M		OVA		Siltstone	23.8	−6.85	−5.98	−2.82	−1.96	1.74	−31.16
OVST 3884	M		OVA		Siltstone	10.7	−2.77	n.d.	−0.45	n.d.	5.87	−31.52
OVST 3887	M		OVA		Micsparite	73.0	−3.19	−2.96	−10.76	−11.14	5.60	−32.23
OVST 3924	M		OVA		Micsparite	76.5	−3.40	−3.20	−6.72	−3.15	1.46	−30.13
OVST 3928	M		OVA		Siltstone	18.4	−3.15	n.d.	−5.79	n.d.	5.15	−32.61
OVST 4224	M		OVA		Siltstone	11.8	−4.62	−3.84	−12.00	−11.58	0.77	−30.82
OVST 4226	M		OVA		Siltstone	28.6	−4.57	−4.76	−11.95	−11.67	0.10	−29.77
OVST 4227	M		OVA		Siltstone	5.5	−2.62	−2.06	−7.57	−5.98	5.39	−31.14
OVST 4234	M		OVA		Siltstone	8.2	−3.58	n.d.	−3.66	n.d.	0.51	−29.42
OVST 4556	M		OVA		Quartzite	14.0	−4.81	−4.67	−7.07	−4.12	1.18	−26.73
OVST 4557	M		OVA		Siltstone	14.6	−2.63	n.d.	−1.50	n.d.	8.32	−31.07
OVST 4560	M		OVA		Sandstone	10.2	−6.76	n.d.	−12.95	n.d.	6.28	−32.35
OVST 4582	M		OVA		Siltstone	36.1	−3.34	−2.50	−12.42	−12.65	2.27	−29.64

[1]Abbreviations used in table are defined in Fig. 2.
n.d. = not determined.

the same strata (cf. Knoll et al., 1986). Fairchild and Spiro (1987) further noted that late diagenetic phases in their Proterozoic carbonates are often volumetrically insignificant. Aharon et al. (1987) also analyzed carbon-isotopic compositions of whole-rock dolomite and dolomicrospar in samples from the late Precambrian Krol Formation of the Lesser Himalaya and found a difference of less than 0.5‰. Evidently, diagenetic shifts of carbon-isotopic abundances in late Proterozoic carbonates are commonly smaller than those in Phanerozoic carbonates (cf. Burdett et al., 1990). This may be related to the low initial porosity of these sediments. Additionally, field and petrographic evidence makes it clear that many Proterozoic carbonate sediments were lithified soon after deposition, with the formation of porosity-occluding cements precipitated from a ground water solution isotopically similar to ambient seawater (Knoll and Swett, 1990).

Whole-rock carbonate is frequently depleted in ^{18}O relative to NLM. The mean difference is 1.0‰, but some much larger depletions are observed. Comparison of ^{13}C and ^{18}O compositions of NLM with those of microsamples of

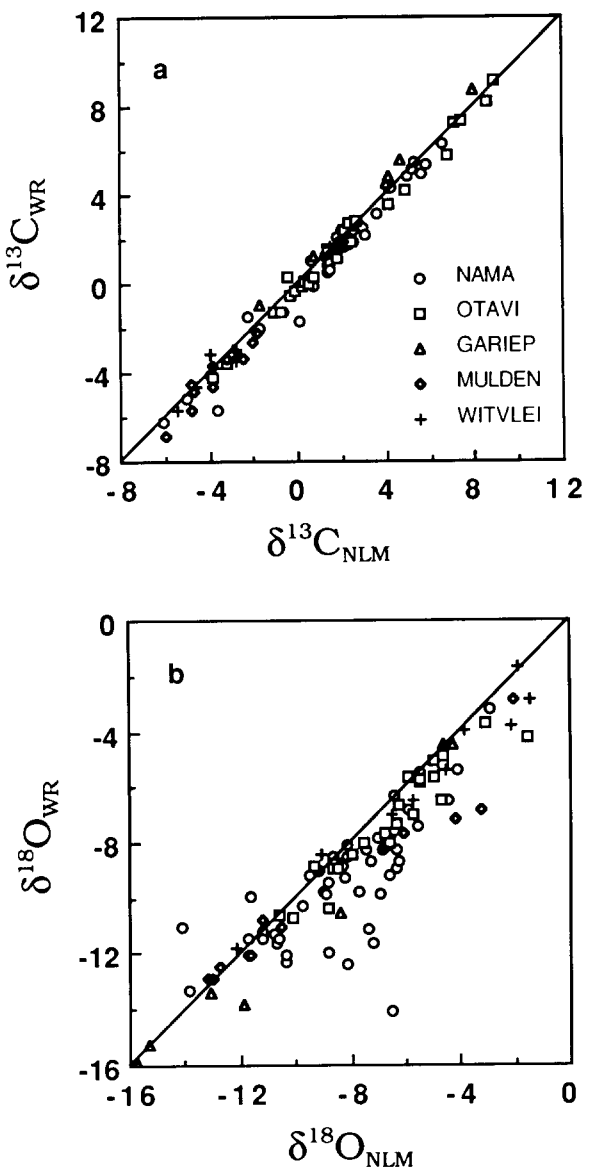

Fig. 7. Crossplots of (a) $\delta^{12}C$ and (b) $\delta^{18}O$ of NLM vs. whole rock carbonate ($n=101$). The line in Fig. 7a and b represent the 1:1 correlation of isotopic abundances of *NLM* and *WR* carbonate.

calcified remains of the Ediacaran grade metazoan *Cloudina* (Grant, 1990) and fine-grained carbonate ooids (Grant and Kaufman, unpublished data) from the same strata indicates that all three phases were precipitated from the same seawater source during Nama times.

Organic carbon

Because dissolved carbonate is in equilibrium with dissolved CO_2, the carbon source utilized by marine primary producers, the isotopic compositions of primary carbonate minerals and sedimentary organic matter are often correlated (e.g., Knoll et al., 1986; Hayes et al., 1989). Close correlation results in a nearly constant value for Δ_B (where B refers to burial of carbon in sediments):

$$\Delta_B = \delta_{carbonate} - \delta_{TOC}$$

The relationship between δ_{TOC}, where TOC is total organic carbon, and δ_{NLM} in the present samples is summarized in Fig. 8. A weak correlation is apparent, but Δ_B is generally smaller than 28.5‰, the value observed in roughly coeval Arctic strata (Knoll et al., 1986), and varies widely. These effects might be attributed either to primary causes, with inputs and biological processing of organic matter differing significantly among samples, or to post-de-

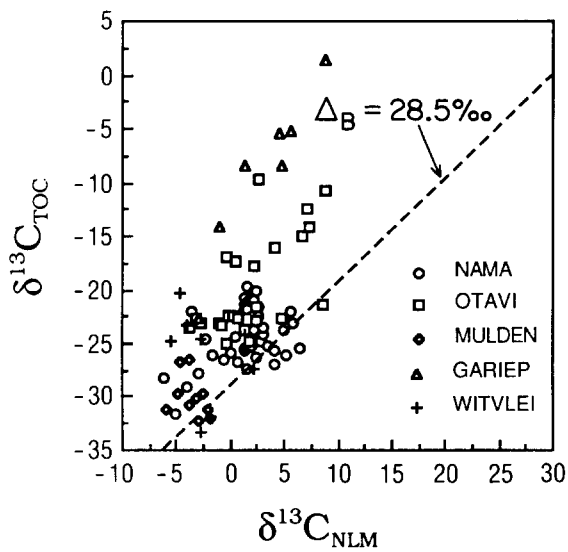

Fig. 8. Crossplot of δ_{TOC} vs. δ_{NLM} ($n=98$). The dashed line represents Δ_B (average carbon-isotopic difference between carbonate and TOC) = 28.5‰, the value observed in a sequence of unmetamorphosed late Proterozoic sediment from Svalbard and East Greenland (Knoll et al., 1986).

TABLE 2

Elemental abundances of Gariep Group kerogens[1]

Sample	N (%)	C (%)	H (%)	N/C	H/C	$\delta^{13}C_{PDB}$[2] (‰)
MV 355	0.42±0.02	93±5	0.30±0.03	0.004±0.001	0.039±0.005	0.9±1.4
MV 364	0.39±0.02	87±4	0.00±0.00	0.004±0.001	0.000±0.000	−5.1±0.4
MV 453	0.22±0.01	32±2	0.84±0.09	0.006±0.002	0.311±0.036	−31.2±0.1
MV 458	0.41±0.09	94±5	1.10±0.11	0.004±0.001	0.141±0.016	−8.4±4
MV 490	0.92±0.05	66±3	0.37±0.04	0.012±0.004	0.067±0.007	−14.2±5
MV 773	0.28±0.02	80±4	0.31±0.03	0.003±0.001	0.047±0.004	−13.9±0.2

[1]Reported values represent means of duplicate measurements. Uncertainties are 95% confidence limits.
[2]CO_2 trapped from effluent of Carlo Erba elemental analyzer.

positional alteration of organic matter. As summarized below, available evidence favors the latter alternative.

The lowest values of Δ_B are observed in samples from the Gariep Group. For six samples, the H/C ratio ranged from 0.00 to 0.31, and averaged 0.10 (Table 2). The H/C ratio of fresh organic matter is near 1.7. The large hydrogen loss required to produce H/C ratios as low as 0.10 is coupled with carbon losses that are so great that the initial isotopic composition of the organic carbon cannot be reconstructed (Hayes et al., 1983). Consequently, the organic-carbon isotopic record in the Gariep Group cannot provide evidence regarding secular trends in the abundance of ^{13}C.

Working upward through the strata examined here, increasing values of Δ_B are observed in the Otavi, Mulden, Witvlei, and Nama groups. Even in the latter two groups, however, $\Delta_B \sim 25‰$, not 28.5‰, and δ_{TOC} does not vary systematically with stratigraphic position. The average concentration of TOC in the Nama and Witvlei groups is only 0.03% ($n=51$ and 13, respectively). In contrast, the average concentration of TOC in the late Proterozoic carbonates from Svalbard and East Greenland (Knoll et al., 1986), in which congruent isotopic variations were observed in carbonates and TOC, was 0.13% ($n=72$). Hayes et al. (1983) have demonstrated that δ_{TOC} tends to increase as concentrations of organic carbon decline. It is likely that the decreased value of Δ_B observed in the Nama and Witvlei groups can be associated with this effect.

Abundances of organic carbon are higher in the Otavi and Mulden groups (averaging respectively 0.13%, $n=40$, and 0.28%, $n=25$), but values of Δ_B tend to lower values and are scattered. These effects are likely related to shearing (Mason, 1981) and heating of these rocks at the time of the Pan-African Orogeny (Clifford, 1967; Kröner et al., 1978). The lowest Δ_B values are observed in Otavi Group samples in which there is textural evidence of alteration, namely, foliated carbonates in the Maieberg and Berg Aukas formations. On balance, we conclude that any record of secular variations in the Damara Supergroup must be based nearly exclusively on the isotopic record in carbonates.

Isotopic variations in carbonate carbon

Nama Group

Secular trends in δ_{NLM} in the Vendian Nama Group (Fig. 9) are dominated by values reaching +6‰ in the Zaris Formation. Lower in the section, values in the Mara Member range from −2 to −6‰. Higher in the section, values average near +2‰. A few samples from reported lagoonal facies (Germs, 1983; Fig. 9) yielded δ_{NLM} values up to 3‰ lower than related open marine samples. However, ^{13}C-depleted carbonates in the Mooifontein Member of the Zaris Formation (samples KMO-5, -6,

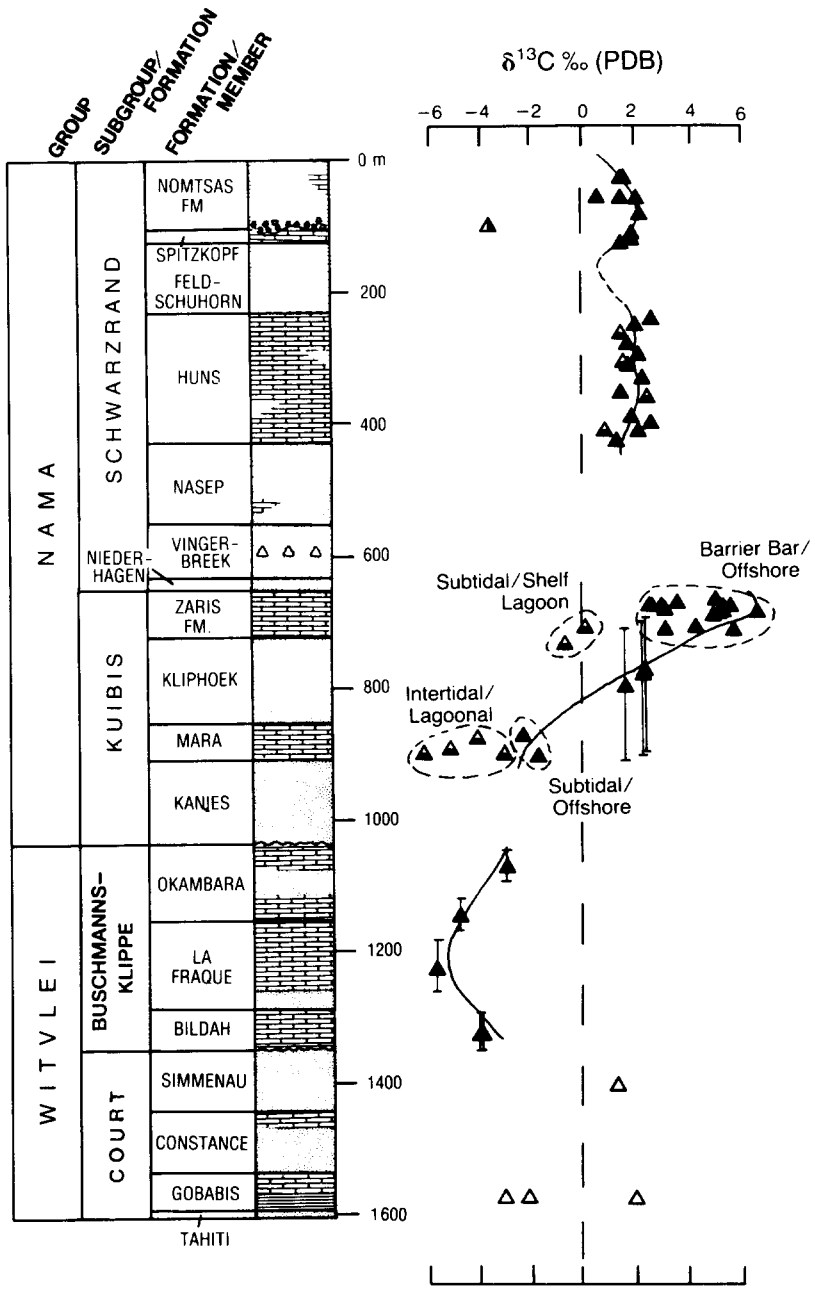

Fig. 9. Stratigraphic column and carbon-isotopic analyses of non-luminescent microspar (NLM) from carbonates in the late Vendian Nama Group, Namibia. Solid symbols represent analyses of NLM samples from marine environments while open symbols represent samples apparently deposited in lacustrine environments. Half-filled (horizontal) symbols represent samples from semi-restricted environments of deposition (Germs, 1983). Half-filled (vertical) symbol represents a silicified sample. Breaks in the curve representing possible secular variations indicate positions of siliciclastic units which were not sampled. Error bars represent stratigraphic uncertainties.

and -8; Table 1) also have significantly reduced carbon-isotopic differences between carbonate and organic carbon ($\Delta\delta^{13}C$ ranges from 25.2 to 26.0‰) relative to other samples from the same member ($\Delta\delta^{13}C$ ranges from 28.4 to 31.8‰). This observation suggest that isotopic compositions of carbonate in the Zaris lagoonal samples have been altered by the reoxidation of organic matter (Irwin et al., 1977). In the Mara Member, $\Delta\delta^{13}C$ values are similar in all samples and, therefore, the ^{13}C-depleted carbonates (samples KM-1, -2, -3, and

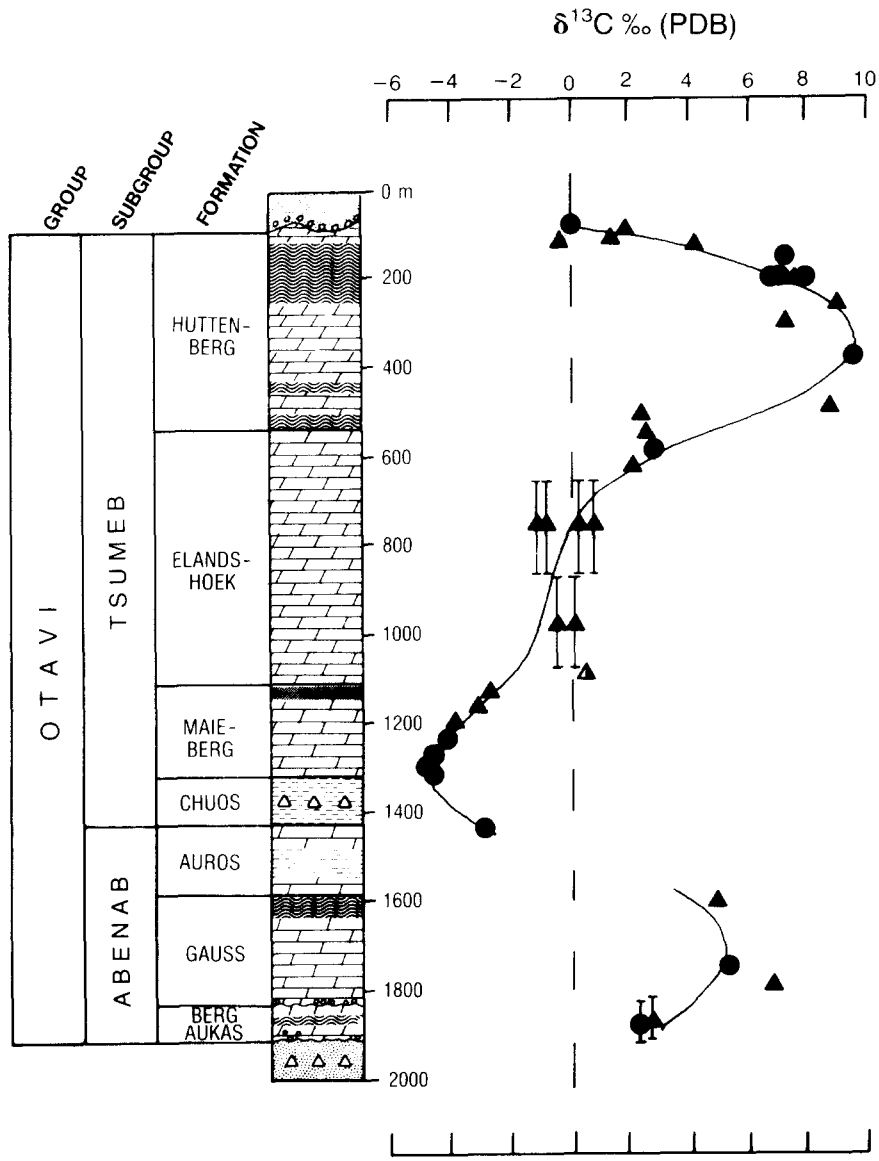

Fig. 10. Stratigraphic column and carbon-isotopic analyses of non-luminescent dolomicrospar and microspar (NLM) in the late Riphean Otavi Group, Namibia. Due to homogeneous grain size and lack of secondary veins, fifteen samples were not subsampled. Whole rock analyses of these samples are indicated by filled circles. Half-filled (vertical) symbol represents a brecciated sample which may have come from lower in the sequence. The break in the curve representing possible secular variations indicates the position of a siliciclastic unit which was not sampled. Error bars represent stratigraphic uncertainties.

-4; Table 1) may reflect true facies variations between precisely equivalent units.

Witvlei Group

Carbonates from the Okamabara, La Fraque, and Bildah members of the Buschmannsklippe Formation are depleted in ^{13}C by 3–6‰ (Fig. 9). Carbonates of possible lacustrine origin from the Court Formation are enriched by approximately 2‰ in the Simmenau and uppermost Constance members and depleted by 2–3‰ in Gobabis Member (with the exception of a stromatolitic sample with $\delta^{13}C = 2.12$‰). The relative stratigraphic positions of samples from the Gobabis Member are unknown.

Otavi Group.

Wide stratigraphic variations in ^{13}C abundances characterize the thick sequence of platform dolomites and limestones in the Otavi Group. Two periods of carbon-isotopic enrichment ($\delta^{13}C > +5$‰) in carbonates of the Gauss and Huttenberg formations are separated by an interval of normal to depleted values in Maieberg and Elandshoek formations (Fig. 10). All of the exceptionally enriched samples in the Huttenberg Formation are dolomites. The relative stratigraphic position of samples from the lower and upper Elandshoek Formation are unknown.

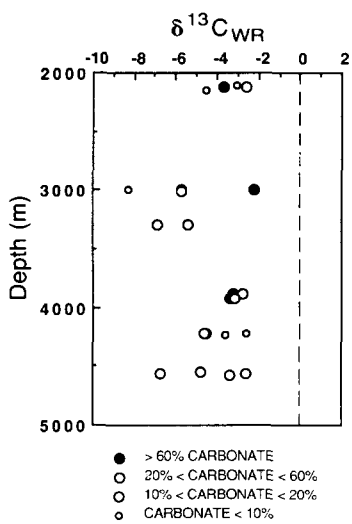

Fig. 11. Carbon-13 abundance of limestones and calcitic siltstones vs. depth in core samples from the Ovamboland Formation of the Mulden Group in Namibia.

Mulden Group

Carbonates in the Ovamboland Formation of the Mulden Group are depleted in ^{13}C, with some δ values ranging as low as −8‰ vs. PDB (Fig. 11). The most depleted values occur in samples which are relatively low in carbonate. Even samples rich in carbonate yield δ values near −3‰, however, and it appears likely that the water body beneath which the Ovamboland Formation formed was characterized by depleted carbon-isotopic abundances.

Gariep Group

Due to lack of stratigraphic control, the availability of only ten samples, and evidence of substantial thermal alteration of organic carbon, secular trends in ^{13}C abundance of total organic carbon cannot be defined. Abundances of ^{13}C in carbonates range from −4 to +8‰ in this group. Two samples from the upper Numees and two samples from the lower Hilda Formations are strongly enriched in ^{13}C, whereas two other samples from the lower Numees Formation as well as samples from the Helskloof, upper Hilda, and Grootderm formations are depleted in ^{13}C (Table 1).

Chemostratigraphic correlations

Interbasinal correlations

Nama Group

The distinctive stratigraphic curve of carbon isotope abundances exhibited by Nama carbonates approximates the major features of curves determined previously for immediately sub-Cambrian successions in Siberia (Magaritz et al., 1986), India (Aharon et al., 1987), and China (Wang et al., 1987): isotopically light carbonates immediately above Varangian tillites are overlain by increasingly ^{13}C enriched limestones, culminating in isotopically

heavy Zaris limestones, above which carbonates are moderately heavy ($\delta^{13}C \sim +2‰$) until the onset of Fish River clastic sedimentation.

Several comments on this pattern seem appropriate:

(1) Allowing for differences in sedimentation rate and stratigraphic continuity, the similarities between Nama carbonates and geographically far removed successions of equivalent age (Fig. 12) strongly suggest that the Vendian isotopic curve determined by several group reflects global seawater history, and, hence, provides data of broad chemostratigraphic and biogeochemical importance.

(2) In light of the above, it is interesting to note that the "Ediacaran excursion" characterizing the Nama Group is not seen in the upper Proterozoic–Cambrian successions of Spitsbergen and East Greenland (Knoll et al., 1986). In these Arctic sections, immediately post-glacial carbonates that are isotopically

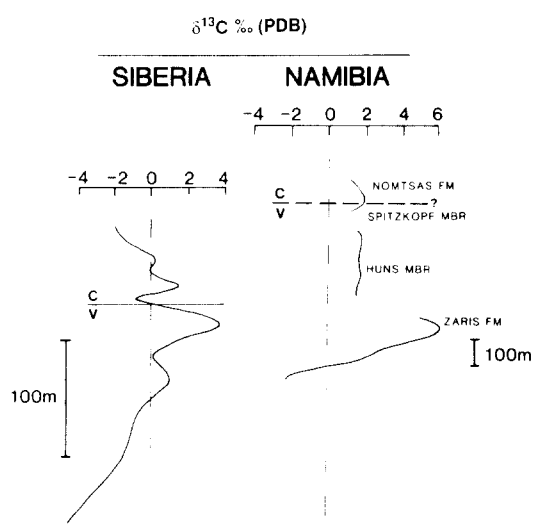

Fig. 12. Comparison of carbon isotope trends in Ediacaran-aged successions from Siberia (Magaritz et al., 1986) and Namibia. Breaks in the curve representing possible secular variations in the Namibian succession indicate siliciclastic units which were not sampled. Position of the Vendian/Cambrian boundary in Siberia is shown as well as the possible position of this boundary in Namibia.

comparable to those of the lower Kuibis Subgroup are overlain by lacustrine sediments (cf. Fairchild and Spiro, 1987) and, above them, Lower Cambrian (Adtabanian) carbonates with $\delta^{13}C$ values of approximately $-1‰$. The absence of an isotopic profile comparable to that of the upper Kuibis and Schwarzrand subgroups is consistent with micropaleontological evidence indicating that the Ediacaran epoch is not represented by marine rocks in eastern Svalbard (Knoll and Swett, 1987).

(3) The Precambrian–Cambrian boundary is not well located in the Nama Group, although if the Cambrian status of *Phycodes pedum* is accepted, the boundary must fall at the base of the Nomtsas Formation (Fig. 12). Use of Siberian sections to constrain this boundary is equivocal – isotopic data require only that the Nomtsas be no older than latest Vendian or younger than earliest Cambrian. Nama data, however, may constrain interpretations of boundary successions in southern Siberia. This region has been considered by many to be a strong candidate for a Precambrian–Cambrian boundary stratotype (e.g., Rozanov, 1984; Rozanov and Sokolov, 1984), but recently Moczydłowska and Vidal (1988) have suggested on the basis of organic-walled microfossils that the Tommotian beds correlate with trilobite-bearing beds in Europe and, hence, are not of basal Cambrian age. The post-Zaris interval of moderately positive $\delta^{13}C$ values characterizing the Huns limestone is absent or strongly condensed in the candidate Precambrian/Cambrian boundary stratotype in Siberian (Magaritz et al., 1986; Fig. 12). Magaritz (1989) reached the same conclusion after finding carbonates with $\delta^{15}C \sim +2‰$ just below the Precambrian/Cambrian boundary in a section 50 km away from the stratotype. Clearly, data from numerous sections will have to be integrated before the detailed pattern of carbon-isotopic variation across the Precambrian–Cambrian boundary can be defined.

Otavi Group

Radiometric age determinations suggest that the Otavi Group should correlate broadly with other upper Riphean successions. The Otavi pattern of strongly positive $\delta^{13}C$ values punctuated by a interval of moderately negative values recalls the pattern observed for 700–800 Ma old carbonates in the Akademikerbreen Group of Svalbard and East Greenland (Knoll et al., 1986) and the Shaler Group of Canada (Hayes et al., unpublished data). The extremely heavy carbonates ($\delta^{13}C > +8‰$) of the upper Otavi Group do not, however, find a match in the Arctic sections. We suspect that the anomalously ^{13}C-enriched carbonates of the Huttenberg Formation reflect the effects of local perturbations. For example, in the Maieberg Formation, dolomites occurring at the top of the sequence are enriched by 3–5‰ relative to siliceous limestones and dolomitic limestones from the same formation. Degens and Epstein (1964) and Land (1980, 1983) suggest that the process of dolomitization in hypersaline, restricted environments can lead to enrichment of ^{13}C over primary values. It is likely that some of the exceptionally high δ_{NLM} values in the present samples derived from this type of enhancement of the Riphean global enrichment (cf. Knoll et al., 1986), and/or other intrabasinal processes.

On the other hand, depletion of ^{13}C greater than $-5‰$ in carbonates from the Maieberg Formation of the Otavi Group (also those from the Mara Member of the Nama Group, the Buschmannsklippe Formation of the Witvlei Group, and the Ovamboland Formation of the Mulden Group) must result from organic matter diagenesis. Mass balance calculations require that authigenic carbonates with $\delta^{13}C < -5‰$ contain some carbon derived from the oxidation of organic matter. In the marine environment, diagenesis of organic carbon and subsequent incorporation of isotopically depleted carbon into carbonates is likely to occur in restricted environments with slow sedimentation rates. However, it should be noted that $\delta^{13}C$ ratios of organic carbon indicate that, relative to subjacent and superjacent strata, these intervals were characterized by ^{13}C depletion.

Intrabasinal correlations

A tentative regional chemostratigraphic correlation of late Proterozoic successions in Namibia is presented in Fig. 13. At present, detailed comparison of secular curves between sequences in the Damara Supergroup is not possible due to low sample density in the Witvlei and Gariep groups. In many instances, therefore, we are restricted to assessing whether isotopic compositions are consistent with independent lithostratigraphic correlations.

On the Kalahari craton, the Vendian Nama Group (Kuibis and Schwarzrand subgroups) lie stratigraphically above the Witvlei and Gariep groups. Although isotopic compositions of carbonates from the lowermost Nama Group and the Buschmannsklippe Formation of the Witvlei Group are similar (Fig. 9), geologic information suggests that these two groups were deposited under significantly different climatic regimes (cf. Germs, 1975) and that the unconformity which separates these groups represents a significant hiatus. On the other hand, the correlation of negative δ values in the Buschmannsklippe Formation with negative δ values in the lower Numees Formation of the Gariep Group is consistent with recent lithostratigraphic evidence for the equivalence of these units (Hoffmann, 1989). Positive δ values ($\delta^{13}C \sim +4‰$) in two samples from the upper Numees Formation can not be correlated with Buschmannsklippe carbonates or any other carbonates of this age in Namibia, and remain problematic. Isotopic compositions of carbonates in the Court Formation (possibly lacustrine) have no clear correlatives on the Kalahari craton, but do fit within the range of values determined for the Hilda Formation.

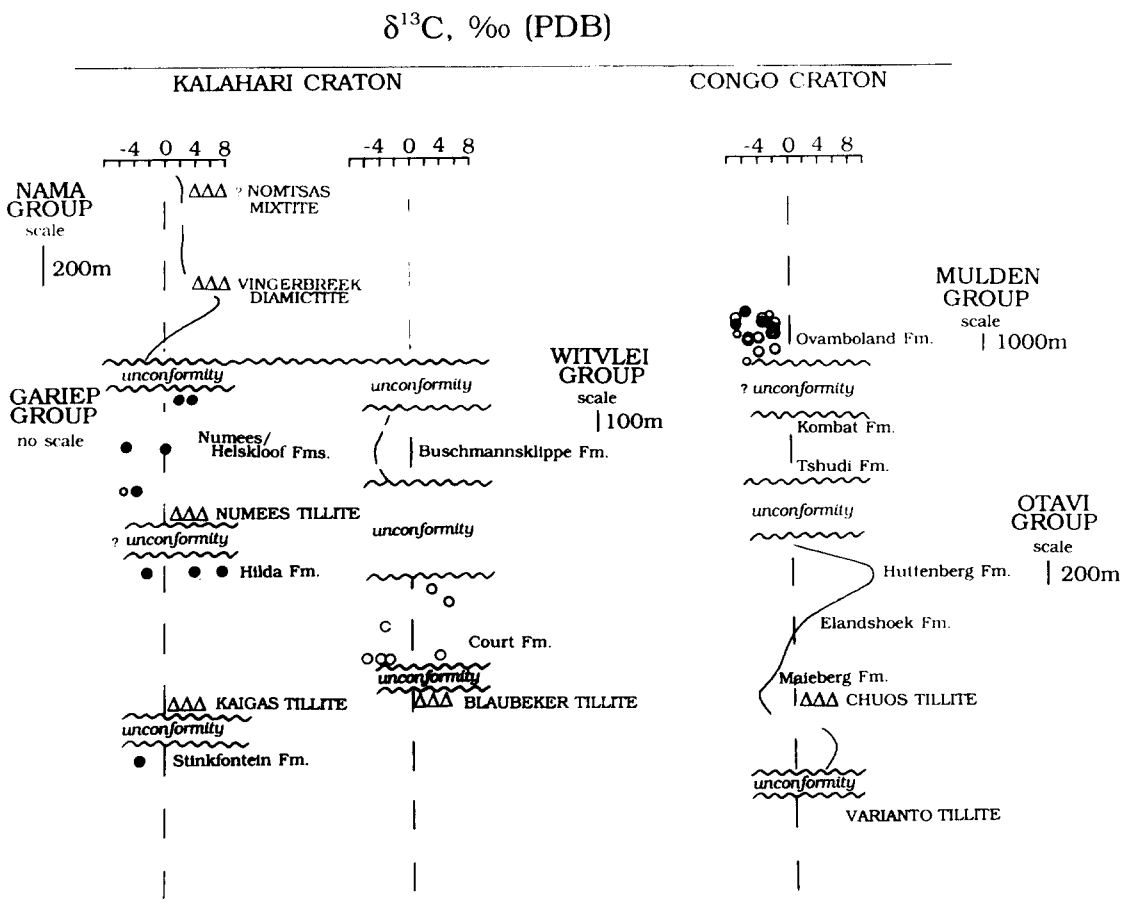

Fig. 13. Correlation between the Nama, Witvlei, Mulden, Otavi, and Gariep groups in Namibia. Symbols used to represent the carbonate abundance of samples in the Mulden and Gariep groups are explained in the legend to Fig. 11. Open symbols in the Court Formation of the Witvlei Group represent reported lacustrine carbonates. Positions of glacigenic units in these late Proterozoic successions are also shown.

On the Congo Craton, negative $\delta^{13}C$ values determined for limestones and calcitic siltstones in the Ovamboland Formation of the Mulden Group can be correlated uniquely with negative $\delta^{13}C$ values determined in limestones from the basal Nama Group (Fig. 13). This correlation fits with the suggestion by Germs (1974) that the Kombat and Tshudi formations below the Ovamboland Formation are older than the Nama Group. Highly positive δ values ($\delta^{13}C > +8‰$) in the Huttenberg and upper Elandshoek formations of the Otavi Group are similar only to highly positive δ values ($\delta^{13}C = +8.7$ and $+5.5‰$) determined for samples from the Hilda Formation in the Gariep Group. Similarly, the range of carbon-isotopic compositions in the lower Elandshoek and Maieberg samples is consistent with values from the Court Formation of the Witvlei Group. These chemostratigraphic data are, therefore, most consistent with the lithostratigraphic correlation of the Chuos, Blaubeker, and Kaigas tillites across the Congo and Kalahari cratons in Namibia.

Late Proterozoic ice ages and iron-formations

In 1986, Knoll et al. noted the stratigraphic correspondence of isotopically light carbonates in Svalbard and East Greenland with Var-

angian glaciogenic strata and hypothesized that late Riphean negative isotopic excursions recorded in the Arctic might reflect pre-Vendian glacial epochs in the Southern Hemisphere. It is interesting that the negative isotopic excursion recorded in the Otavi Group indeed corresponds to the deposition of the Chuos tillite (Fig. 10). In fact, if the proposed intrabasinal chemostratigraphy is correct, negative isotopic excursions are correlated with three separate glaciations in Namibia, represented by (1) the Chuos–Blaubeker–Kaigas tillites; (2) the Numees tillite; and (3) the Vingerbreek diamictite stratigraphically above the Zaris Formation in the Nama Group (Fig. 13). This correspondence of glacial phenomena and negative isotopic excursions may reflect lowered sea levels, invigorated circulation of O_2-rich bottom water, and the erosion of coastal organic-rich sediments during glacial periods (Knoll, in press).

Also associated with the Chuos Formation are hematitic and magnetitic sedimentary iron-formation (Hedberg, 1979). Young (1976) first noted a global correlation of late Proterozoic glacial horizons with iron-formations. We add that there is a further correlation of this phenomenon with carbon-isotopic depletion. The association of ^{13}C-depleted carbonates, iron-formation, and glacial sediments is also evident in the Proterozoic sediments from the Adelaide Geosyncline of South Australia (Donnelly, 1981; Williams, 1981; Knutson et al., 1983).

To explain these correlations we must try to interrelate primary changes in the isotopic composition of sedimentary carbon with the remarkable appearance of iron-formations after a depositional hiatus of approximately 1 Ga and glacial phenomena. Primary shifts in the ^{13}C composition of water column carbonate in the world oceans may be forced by changing ocean circulation patterns, continental configuration, and degree of seafloor spreading, all of which can alter the fraction of organic carbon preserved in ocean sediments. Enhanced burial of organic carbon causes enrichment of carbon-13 in carbonates (Broecker, 1970; Scholle and Arthur, 1980). Conversely, decreasing the fraction of carbon buried in organic form leads to depletion of ^{13}C in marine carbonate.

Isotopic variations summarized by Knoll et al. (1986) and in this study show that prior to the extensive low latitude glaciation represented by the Chuos Formation tillites, conditions favored globally enhanced burial of organic carbon. It is likely that marine waters were stratified, with deep layers anoxic. A prolonged period of anoxic conditions in the deep ocean would allow for the buildup of large quantities of ferrous iron (Holland, 1973, 1984) probably sourced from hydrothermal inputs (Veizer, 1983; Yeo, 1984; Shaw and Wasserburg, 1985; Derry and Jacobsen, 1988; Derry et al., 1989). At the onset of worldwide glaciation, burial of organic carbon would decrease due to (1) lowering of sealevel; (2) decrease in the areal distribution of stable platforms due to extensive ice cover; and (3) enhanced ventilation of the oceans due to strong thermal gradients (Broecker, 1981, 1982; Curry et al., 1988; Knoll, in press). Upwelling forced by invigorated deep circulation would bring ^{13}C-depleted and iron-rich anoxic bottom waters onto the shallow shelves where contact with cold, oxygenated surface waters would lead to the precipitation of iron-formation (Martin, 1965; Yeo, 1984).

Conclusions

Reduced and variable values for Δ_B, coupled with extensive dehydrogenation and textural evidence of thermal or deformational events, indicate that isotopic compositions of organic carbon in upper Proterozoic sedimentary rocks from Namibia have been altered significantly. Carbon-isotopic compositions of whole-rock carbonates and of microsampled, non-luminescent microspar and dolomicrospar are nearly equal, although oxygen-isotopic com-

positions often differ significantly. In both cases, microspar is enriched in the heavy isotope relative to whole-rock values. The most enriched $\delta^{18}O$ values approach $-3‰$ vs. PDB, at best establishing a minimum value for the ^{18}O content of late Proterozoic seawater.

Secular variations in ^{13}C abundances of carbonates in the Nama and Otavi groups cannot be ascribed to diagenetic or metamorphic effects, and, in concert with lithostratigraphic determinations, provide a useful constraint on correlation with the Damara Supergroup. General stratigraphic patterns of variation are similar to those previously determined for other, widely separated late Proterozoic basins, increasing our confidence that patterns of secular variation in $\delta^{13}C$ reflect global changes in the isotopic composition of late Proterozoic seawater, a conclusion of both chemostratigraphic and biogeochemical importance. The deposition of late Proterozoic iron-formations may be associated with the disturbance of anoxic bottom waters, especially in extensional basins where the hydrothermal input of ferrous iron may have been relatively high. The correlation of both iron-formation and glaciogenic deposits with distinct oscillations in $\delta^{13}C$ is consistent with such a scenario.

Acknowledgements

Earlier versions of this paper were improved by discussions with B. Popp, T. Donnelly, I. Lambert, P. Aharon, J. McKenzie, H. Strauss, and S. Grant as well as reviews by M. Schildlowski, K. Eriksson, and I. Fairchild. We thank the Geological Survey of Namibia, the Tsumeb Corporation, J. Compton, M.V. von Veh, and W. Hegenberger for the donation of samples. Thanks also go to S. Studley for technical assistance, J. Tolens of the Indiana Geological Survey for drafting, and to K. Hoffmann for some of the lithostratigraphic correlations between sediments on the Kalahari Craton. Research was supported in part by grants from NASA (NGR 15-003118 to J.M.H. and NAGW-893 to A.H.K.).

References

Aharon, P., Schidlowski, M. and Singh, I.B., 1987. Chronostratigraphic markers in the end-Precambrian carbon isotope record of the lesser Himalaya. Nature, 327: 699–702.

Ahrendt, H., Hunziker, J.C. and Weber, K., 1978. Age and degree of metamorphism and time of nappe emplacement along the southern margin of the Damara Orogen, Namibia (S.W.A.). Geol. Rundsch., 67: 719–742.

Allsopp, H.L., Kostlin, E.O., Welke, H.H., Burger, A.J., Kröner, A. and Blignault, H.J., 1979. Rb–Sr and U–Pb geochronology of late Precambrian–Early Paleozoic igneous activity in the Richtersveld (South Africa) and southern South West Africa. Trans. Geol. Soc. S. Afr., 82: 185–204.

Brand, U. and Veizer, J., 1980. Chemical diagenesis of a multicomponent system – I. Trace elements. J. Sediment. Petrol., 50: 1219–1236.

Brand, U. and Veizer, J., 1981. Chemical diagenesis of a multicomponent system – II. Stable isotopes. J. Sediment. Petrol., 51: 987–998.

Broecker, W.S., 1970. A boundary condition on the evolution of atmospheric oxygen. J. Geophys. Res., 75: 3553–3557.

Broecker, W.S., 1981. Geochemical tracers and ocean circulation. In: B.A. Warren and C. Wunsch (Editors), Evolution of Physical Oceanography. MIT Press, Cambridge, MA, pp. 434–460.

Broecker, W.S., 1982. Glacial to interglacial changes in ocean chemistry. Prog. Oceanogr., 11: 151–197.

Burdett, J.W., Grotzinger, J.P. and Arthur, M.A., 1990. Did major changes in the stable-isotope composition of Proterozoic seawater occur? Geology, 18: 227–230.

Clifford, T.N., 1967. The Damaran episode in the upper Proterozoic–Lower Paleozoic structural history of Southern Africa. Geol. Soc. Am. Spec. Pap., 92, 100 pp.

Crimes, T.P., 1987. Trace fossils and correlation of late Precambrian and early Cabrian stata. Geol. Mag., 124: 97–119.

Crimes, T.P. and Germs, G.J.B., 1982. Trace fossils from the Nama Group (Precambrian–Cambrian) of South West Africa/Namibia. J. Paleontol., 65: 890–907.

Curry, W.B., Duplessy, J.C., Labeyrie, L. and Shackleton, N.J., 1988. Changes in the distribution of $\delta^{13}C$ of deep water ΣCO_2 between the last glaciation and the Holocene. Paleoceanography, 3: 317–341.

Degens, E.T. and Epstein, S., 1964. Oxygen and carbon isotope ratios in coexisting calcites and dolomites from recent and ancient sediments. Geochim. Cosmochim. Acta, 28: 23–44.

Derry, L. and Jacobsen, S., 1988. The Nd and Sr isotopic evolution of Proterozoic seawater. Geophys. Res. Lett., 15: 397–400.

Derry, L., Keto, L.S., Jacobsen, S., Knoll, A.H. and Swett, K., 1989. Sr isotopic variations of upper Proterozoic carbonates from East Greenland and Svalbard. Geochim. Cosmochim. Acta, 53: 2331–2339.

De Villiers, J., 1968. Fifth Ann. Rept., Precambrian Res. Unit, Univ. Cape Town, p. 39–40.

Dickson, J.A.D., 1966. Carbonate identification and genesis as revealed by staining. J. Sediment. Petrol., 12: 133–149.

Donnelly, T.H., 1981. Discussion: Sedimentology, stable-isotope geochemistry and paleoenvironment of dolostones capping late Precambrian glacial sequences in Australia. J. Geol. Soc. Aust., 28: 99–101.

Fairchild, I.J. and Spiro, B., 1987. Petrological and isotopic implications of some contrasting late Precambrian carbonates, N.E. Spitsbergen. Sedimentology, 34: 973–989.

Fairchild, I.J., Hendy, G., Quest, M. and Tucker, M., 1988. Chemical analysis of sedimentary rocks. In: M. Tucker (Editor), Techniques in Sedimentology, Blackwell, Oxford, pp. 274–354.

Frets, D.C., 1969. Geology and structure of the Huab–Welwitschia area, South West Africa. Bull. Precambrian Res. Unit, Univ. Cape Town, 5: 235 pp.

Germs, G.J.B., 1972a. The stratigraphy and paleontology of the lower Nama Group, South West Africa. Bull. Precambrian Res. Unit, Univ. Cape Town, 12: 250 pp.

Germs, G.J.B., 1972b. New shelly fossils from the Nama Group, South West Africa. Am. J. Sci., 272: 752–761.

Germs, G.J.B., 1972c. Trace fossils from the Nama Group, South West Africa. J. Paleontol., 46: 864–876.

Germs, G.J.B., 1973a. A reinterpretation of *Rangea schneiderhoehni* and the discovery of a related new fossil from the Nama Group, South West Africa. Lethaia, 6: 1–10.

Germs, G.J.B., 1973b. Possible sprigginid worms and a new trace fossil from the Nama Group, South West Africa. Geology, 1: 69–70.

Germs, G.J.B., 1974. The Nama Group in South West Africa and its relationship to the Pan-African geosyncline. J. Geol., 82: 301–317.

Germs, G.J.B., 1975. Silicification structures from the upper Otavi Group and the significance of chert in this unit. Trans. Geol. Soc. S. Afr., 78: 67–70.

Germs, G.J.B., 1983. Implications of a sedimentary facies and depositional environmental analysis of the Nama Group in South West Africa/Namibia. Geol. Soc. S. Afr. Spec. Publ., 11: 89–114.

Germs, J.B.G., Knoll, A.H. and Vidal, G., 1986. Latest Proterozoic microfossils from the Nama Group, Namibia (South West Africa). Precambrian Res., 32: 45–62.

Glaessner, M.F., 1963. Zur Kenntnis der Nama-Fossilien Südwest-Afrikas. Ann. Natushist. Mus. Wein, 66: 113–120.

Glaessner, M.F., 1978. Re-examination of *Archaeichnium*, a fossil from the Nama Group. Ann. S. Afr. Mus., 74: 335–342.

Glaessner, M.F., 1979. An echiurid worm from the late Precambrian. Lethaia, 12: 121–124.

Glaessner, M.F., 1984. The Dawn of Animal Life: a Biohistory Study. Cambridge Univ. Press, Cambridge, 224 pp.

Grant, S.W.F., 1990. Shell structure and distribution of *Cloudina*, a potential index fossil for the terminal Proterozoic. Am. J. Sci., 290A: 261–294.

Grant, S.W.F., Knoll, A.H. and Germs, J.G.B., in press. A probable calcified metaphyte in the latest Proterozoic Nama Group, Namibia: Its origin, diagenesis and implications. J. Paleontol., 65.

Gross, M.G., 1964. Variations in the $^{18}O/^{16}O$ and $^{13}C/^{12}C$ ratios of diagenetically altered limestones in the Bermuda Islands. J. Geol., 72: 170–194.

Gürich, G., 1930. Die bislang ältesten Spuren von Organismen in Süd-Afrika. C.R. 15th. Int. Geol. Congr., S. Afr., 1929: 670–680.

Gürich, G., 1933. Die Kuibis-Fossilien der Nama Formation von Südwest-Afrika. Paleontol. Z., 15: 137–154.

Hayes, J.M., Kaplan, I.R. and Wedeking, K.W., 1983. Precambrian organic geochemistry, preservation of the record. In: J.W. Schopf (Editor), Earth's Earliest Biosphere. Its Origin and Evolution. Princeton Univ. Press, Princeton, NJ, pp. 93–134.

Hayes, J.M., Popp, B.N., Takagiku, R. and Johnson, M.W., 1989. An isotopic study of biogeochemical relationships between carbonates and organic carbon in the Greenhorn Formation. Geochim. Cosmochim. Acta, 53: 2961–2972.

Hedberg, R.M., 1979. Stratigraphy of the Ovamboland basin, South West Africa. Bull. Precambrian Res. Unit, Cape Town, 24: 325 pp.

Hemming, N.G., Meyers, W.J. and Grams, J.C., 1989. Cathodoluminescence in diagenetic calcites: The role of Fe and Mn ans deduced from electron probe and spectrophotometric measurements. J. Sediment. Petrol., 59: 404–411.

Hoffmann, K.H., 1989. New aspects of lithostratigraphic subdivision and correlation of late Proterozoic to early Cambrian rocks of the southern Damara Belt and their correlation with the central and northern Damara Belt and the Gariep Belt. Commun. Geol. Serv. Namibia, 5: 59–67.

Holland, H.D., 1973. The oceans: A possible source of iron in iron-formations. Econ. Geol., 68: 1169–1172.

Holland, H.D., 1984. The Chemical Evolution of the Atmosphere and Oceans. Princeton Univ. Press, Princeton, NJ, 582 pp.

Holser, W.T., 1984. Gradual and abrupt shifts in ocean

chemistry during Phanerozoic time. In: H.D. Holland and A.F. Trendall (Editors), Patterns of Change in Earth Evolution. Springer, Berlin, pp. 123–144.

Holser, W.T., Magaritz, M. and Wright, J., 1986. Chemical and isotopic variations in the world ocean during the Phanerozoic. In: O. Walliser (Editor), Global Bio-Events. Springer, Berlin, pp. 63–74.

Horstmann, U.E., Ahrendt, H., Clauer, N. and Porada, H., 1990. The metamorphic history of the Damara Orogen based on K/Ar data of detrital white micas from the Nama Group, Namibia. Precambrian Res., 48: 41–61.

Irwin, H., Curtis, C. and Coleman, M., 1977. Isotopic evidence for source of diagenetic carbonates formed during burial of organic-rich sediments. Nature, 269: 209–213.

Jacob, R.E., 1974. Geology and metamorphic petrology of the southern margin of the Damara Orogen around Omitara, southwest Africa. Bull. Precambrian Res. Unit, Univ. Cape Town, 17: 185 pp.

Keith, M.L. and Weber, J.N., 1964. Carbon and oxygen isotopic compositions of selected limestones and fossils. Geochim. Cosmochim. Acta, 28: 1787–1816.

Knoll, A.H., in press. Biological and biogeochemical preludes to the Ediacaran radiation. In: J.H. Lipps and P.W. Signor (Editors), Origins and Early Evolutionary History of the Metazoan. Plenum, New York, NY.

Knoll, A.H. and Swett, K., 1987. Micropaleontology across the Precambrian–Cambrian boundary in Spitsbergen. J. Paleontol., 61: 898–926.

Knoll, A.H. and Swett, K., 1990. Carbonate deposition during the late Proterozoic era: An example from Spitzbergen. Am. J. Sci., 290A: 104–132.

Knoll, A.H., Hayes, J.M., Kaufman, A.J., Swett, K. and Lambert, I.B., 1986. Secular variation in carbon isotope ratios from Upper Proterozoic successions of Svalbard and East Greenland. Nature, 321: 832–838.

Knutson, J., Donnelly, T.H. and Tonkin, D.G., 1983. Geochemical constraints on the genesis of copper mineralization in the Mount Gunson Area, South Australia. Econ. Geol., 78: 250–274.

Kröner, A., 1971. Late Precambrian correlation and the relationship between the Damara and Nama Systems of South West Africa. Geol. Rundsch., 60: 1513–1523.

Kröner, A. and Germs, G.J.B., 1971. A re-interpretation of the Numees–Nama contact at Aussenkjer, South West Africa. Trans. Geol. Soc. S. Afr., 74: 69–74.

Kröner, A., Halpern, M. and Jacob, R.E., 1978. Rb–Sr geochronology in favour of polymetamorphism in the Pan African Damara Belt of Namibia (South West Africa). Geol. Rundsch., 67: 688–705.

Kröner, A., McWilliams, M.O. Germs, G.J.B., Reid, A.B. and Schalk, K.E.L., 1980. Paleomagnetism of late Precambrian to early Paleozoic mixtite-bearing formations in Namibia (South West Africa): The Nama Group and Blaubeker Formation. Am. J. Sci., 280: 942–968.

Kruger, L., 1969. Stromatolites and oncolites in the Otavi Series, South West Africa. J. Sediment. Petrol., 39: 1046–1056.

Lambert, I.B., Walter, M.R., Zang Wenglong, Lu Songnian and Ma Guogan, 1987. Paleoenvironment and carbon isotope stratigraphy of upper Proterozoic carbonates of the Yangtze Platform. Nature, 325: 140–142.

Land, L.S., 1980. The isotopic and trace element geochemistry of dolomite: The state of the art. In: D.H. Zenger, J.B. Dunham and R.L. Ethington (Editors), Concepts and Models of Dolomitization. SEPM Spec. Publ. 28: 87–110.

Land, L.S., 1983. The application of stable isotopes to studies of the origin of dolomite and to problems of diagenesis of clastic sediments. In: M.A. Arthur, T.F. Anderson, I.R. Kaplan, J. Veizer and L.S. Land (Editors), Stable Isotopes in Sedimentary Geology. SEPM Short Course, 10: 4.1–4.22.

Lindh, T.B., 1983. Temporal variations in ^{13}C, ^{34}S and global sedimentation during the Phanerozoic. Thesis. Univ. Miami, FL, 98 pp. (unpublished).

Lombaard, A.F., Gunzel, A., Innes, J. and Kruger, L., 1986. The Tsumeb lead–copper–zinc–silver deposits, South West Africa/Namibia. In: C.R. Anhaeusser and S. Maske (Editors), Mineral Deposits of Southern Africa. Geol. Soc. S. Afr., Johannesburg, pp. 1761–1787.

Magaritz, M., 1989. ^{13}C minima follow extinction events: A clue to faunal radiation. Geology, 17: 337–340.

Magaritz, M., Holser, W.T. and Kirschvink, J.L., 1986. Carbon isotope events across the Precambrian/Cambrian boundary on the Siberian Platform. Nature, 320: 258–259.

Martin, H., 1965. The Precambrian geology of South West Africa and Namaqualand. Bull. Precambrian Res. Unit, Univ. Cape Town, 159 pp.

Mason, R., 1981. The Damara mobile belt in South West Africa/Namibia. In: D.R. Hunter (Editor), Precambrian of the Southern Hemisphere. Elesevier, Amsterdam, 882 pp.

McCrea, J.M., 1950. On the isotopic chemistry of carbonates and a paleotemperature scale. J. Chem. Phys., 18: 849–857.

McMillan, M.D., 1968. Geology of the Witputs–Sendelingsdrif area. Bull. Precambrian Res. Unit, Univ. Cape Town, 4: 177 pp.

Miller, R.McG., 1983. The Pan-African Damara Orogen of South West Africa/Namibia. Geol. Soc. S. Afr. Spec. Publ., 11: 431–515.

Miller, R.McG. and Burger, A.J., 1983. U–Pb zircon age of the early Damaran Naauwpoort Formation. Geol. Soc. S. Afr. Spec. Publ., 11: 267–272.

Moczydłowska, M. and Vidal, G., 1988. How old is the Tommotian? Geology, 16: 166–168.

Narbonne, G.M. and Myrow, P., 1988. Trace fossil biostratigraphy in the Precambrian–Cambrian boundary interval. N.Y. State Mus. Bull., 463: 72–76.

Pflug, H.D., 1966. Neue Fossilreste aus den Nama-Schichten in Südwest-Afrika. Paläontol. Z., 40: 14–25.

Pflug, H.D., 1970a. Zur Fauna der Nama-Schichten in Südwest-Afrika. I. Pteridinia, Bau und systematische Zugehörigkeit. Palaeontographica, Abt. A., 134: 153–262.

Pflug, H.D., 1970b. Zur Fauna der Nama-Schichten in Südwest-Afrika. II. Rangeidae, Bau und systematische Zugehörigkeit. Palaeontolgraphica, Abt. A., 135: 198–231.

Pflug, H.D., 1972. Zur Fauna der Nama-Schichten in Südwest-Afrika. III. Erniettomorpha, Bau und Systematik. Palaeontographica, Abt. A., 139: 134–170.

Pflug, H.D., 1973. Zur Fauna der Nama-Schichten in Südwest-Afrika. IV. Mikroskopische Anatomie der Petalo-Organismen. Palaeontographica, Abt. A., 144: 166–202.

Porada, H., 1989. Pan-African rifting and orogenesis in southern to equatorial Africa and eastern Brazil. Precambrian Res., 44: 103–136.

Richter, R., 1955. Die ältesten Fossilien Süd-Afrikas. Senckenbergiana Lethaea, 36: 243–289.

Rosenbaum, J. and Sheppard, S.M.F., 1986. An isotopic study of siderites, dolomites and ankerites at high temperatures. Geochim. Cosmochim. Acta, 50: 1147–1150.

Rozanov, A.Yu., 1984. The Precambrian/Cambrian boundary in Siberia. Episodes, 7: 20–24.

Rozanov, A.Yu. and Sololov, B.S., 1984. Lower Cambrian stage subdivision stratigraphy. Nauka, Moscow, 184 pp. (in Russian).

Sandberg, P.A., 1983. An oscillating trend in Phanerozoic non-skeletal carbonate mineralogy. Nature, 305: 19–22.

Sandtrock, J., Studley, S.A. and Hayes, J.M., 1985. Isotopic analyses based on the mass spectrum of carbon dioxide. Anal. Chem., 57: 1444–1448.

Schidlowski, M., Eichmann, R. and Junge, C., 1975. Precambrian sedimentary carbonates: Carbon and oxygen isotope geochemistry and implications for the terrestrial oxygen budget. Precambrian Res., 2: 1–69.

Scholle, P.A. and Arthur, M.A., 1980. Carbon isotope fluctuations in Cretaceous pelagic limestones: Potential stratigraphic and petroleum exploration tool. Bull. Am. Assoc. Pet. Geol, 64: 67–87.

Shaw, H.F. and Wasserburg, G.J., 1985. Sm–Nd in marine carbonates and phosphates: Implications for Nd isotopes in seawater and crustal ages. Geochim. Cosmochim. Acta, 49: 503–518.

Smith, D.A.M., 1961. The geology of the area around the Khan and Swakop Rivers in South West Africa. Thesis. Univ. Witswatersrand, Johannesburg, 77 pp.

Söhnge, P.G., 1964. The geology of the Tsumeb mine. Geol. Soc. S. Afr. Spec. Publ., 2: 367–382.

Swett, K. and Knoll, A.H., 1989. Marine pisoliths from upper Proterozoic carbonates of East Greenland and Spitsbergen. Sedimentology, 36: 75–93.

Tankard, A.J., Hobday, D.K., Jackson, M.P.A., Hunter, D.R., Eriksson, K.A. and Minter, W.E., 1982. The Crustal Evolution of Southern Africa. Springer, New York, NY, 523 pp.

Tucker, M.E., 1983. Sedimentation of organic-rich limestones in the late Precambrian of southern Norway. Precambrian Res., 22: 293–315.

Tucker, M.E., 1985. Calcitized aragonite ooids and cements from the late Precambrian Biri Formation of southern Norway. Sediment. Geol., 43: 67–84.

Tucker, M.E., 1986a. Carbon isotope excursions in Precambrian/Cambrian boundary beds, Morocco. Nature, 319: 48–50.

Tucker, M.E., 1986b. Formerly aragonitic limestones associated with tillites in the late Proterozoic of Death Valley, California. J. Sediment. Petrol., 56: 818–830.

Veizer, J., 1978. Secular variations in the composition of sedimentary carbonate rocks, II. Fe, Mn, Ca, Mg, Si and minor constituents. Precambrian Res., 6: 318–413.

Veizer, J., 1983. Chemical diagenesis of carbonates: Theory and application. In: M.A. Arthur, T.F. Anderson, I.R. Kaplan, J. Veizer and L.S. Land (Editors), Stable Isotopes in Sedimentary Geology. S.E.P.M. Short Course No. 10: 3.1–3.100.

Veizer, J. and Hoefs, J., 1976. The nature of $^{18}O/^{16}O$ and $^{13}C/^{12}C$ secular trends in sedimentary rocks. Geochim. Cosmochim. Acta, 40: 1387–1395.

Veizer, J., Holser, W.T. and Wilgus, C.K., 1980. Correlation of $^{13}C/^{12}C$ and $^{34}S/^{32}S$ secular variations. Geochim. Cosmochim. Acta, 44: 579–587.

Wachter, E.A. and Hayes, J.M., 1985. Exchange of oxygen isotopes in carbon dioxide phosphoric acid systems. Chem. Geol. (Isot. Geosci. Sect.), 52: 365–374.

Wang, F., Liu, R. and Zhao, D., 1987. Precambrian stromatolite oxygen isotopes from Sichuan–Yunnan area and its significance. Bull. Chengdu Inst. Geol. Min. Res., 8: 61–68.

Wedeking, K.W., Hayes, J.M. and Matzigkeit, U., 1983. Procedures of organic geochemical analysis. In: J.W. Schopf (Editor), Earth's Earliest Biosphere: Its Origin and Evolution. Princeton Univ. Press, Princeton, NJ, pp. 428–440.

Welke, H.J., Burger, A.J., Corner, B., Kröner, A. and Blignault, H.J., 1979. U–Pb and Rb–Sr age determinations on Middle Proterozoic rocks from the lower Orange River area, southwestern Africa. Trans. Geol. Soc. S. Afr., 82: 205–214.

Williams, G.E., 1981. Reply: Sedimentology, stable-isotope geochemistry and paleoenvironment of dolostones capping late Precambrian glacial sequences in Australia. J. Geol. Soc. Aust., 28: 102–105.

Yeo, G., 1984. The Rapitan Group: Relevance to the global association of late Proterozoic glaciations and iron-formation. Thesis. Univ. W. Ontario, London, Ont.

Young, G.M., 1976. Iron-formation and glaciogenic rocks of the Rapitan Group, Northwest Territories. Precambrian Res., 3: 137–158.

Zempolich, W.G., Wilkinson, B.H. and Lohmann, K.C., 1988. Diagenesis of late Proterozoic carbonates: The Beck Springs Dolomite of eastern California. J. Sediment. Petrol., 58: 656–672.